Doctoral Dissertation

A study on modular robots with multi-directional movement

Mak Kwan Wai

January, 2020

Graduate School of Engineering
Osaka University

Abstract

This thesis discusses the idea of developing a new modular robot, which can achieve high freedom of movement, couple with other robots and perform synchronized actions, for the construction of locomotive structures in micro gravity environment.

First, a new design of cubic robot (Macrotis) using snap-through-buckling mechanisms as actuators was proposed for achieving high freedom of movement. By installing two snap-through-buckling mechanisms on the robot, together with other mechanisms for adjusting the directions of force output, a translational force can be generated when the two mechanisms generate forces at the same time to the same direction; a moment about the center of the robot can be generated when those forces are in the opposite directions. In addition, the 2 platforms can be aligned with the horizontal level when the robot is positioned horizontally on ground in any orientation. The robot's movement can be controlled through suitable electronic and software design. The motions of the robot under micro gravity was demonstrated by performing experiment on a slope, where the force component parallel to the surface of the slope acted as the pseudo micro gravitational force. In the experiment, rolling and jumping motions of the robot were assessed.

Second, a wireless multi-master communication platform for distributed robot systems was developed. Cube-shaped, transparent test modules with infra-red (IR) transceivers installed at all 6 faces were produced. Each test module is equipped with an electronic circuit for supporting wireless transmission of CAN messages via IR, with two rules introduced to the circuit to avoid formation of deadlock loop, regardless of the formation of modules. Messages are prioritized using unique identifiers (ID) offered to all modules. Relay of messages by modules was promoted by modifying the ID field. A program was designed to test on the communication platform, where the periodic LED flash of modules were to be synchronized through communication between modules. From experiments, it is verified that communication can be established and synchronization can be achieved with 8 modules in 4 different formations. The very small deviation in absolute time difference in the flash of modules shows that modules can be well synchronized by using the communication platform.

Third, a new cubic modular robot that consists of the actuator part of Macrotis and a magnet-equipped body frame was considered. With the design, it is supposed that the robot is capable of performing jumping and rolling motions in multiple directions, and coupling with other robots for forming closely packed structures. Based on the information obtained from the distance sensors installed on all faces of the body frame for measuring the distance between robots, and the sensor for detecting the direction of gravity, rules were set for controlling the action of robots. With parameters of Macrotis applied and equations implemented for resolving force and torque acting on magnets in the field, a computer simulation was conducted using Open Dynamics Engine. Through simulation conducted with cases of different initial position and orientation on different number of robots in the field, statistical results show that the average number of clusters formed, average number of robots included in the largest cluster formed and the time for forming the structures increase with the number of robots in the field.

Acknowledgements

I would like to express my sincere gratitude to my supervisor, Prof. Koichi Osuka, who gave me a chance to study for a doctoral degree, and aroused my interest in academic research. I am respectful for his enthusiasm in research, which has provided a lot of inspiration and valuable guidance on my research. He is a kind, friendly and open-minded person, who always encourage me and listen to me. I truly appreciate Assoc. Prof. Yasuhiro Sugimoto and Assoc. Prof. Teruyo Wada for their constructive advice and tremendous support in editing papers. I am deeply thankful to Prof. Masato Ishikawa and Assoc. Prof. Yuki Minami, for the experience they shared and their encouragement, which gave me confidence in conducting research. I would like to thank Prof. Mitsuru Higashimori for providing his precious time as my committee member. I would like to thank Asst. Prof. Yuichiro Sueoka for having interesting conversations with me.

Many thanks to Mr. Youji Miyake and Mr. Genki Yamasaki, the technicians who offered a lot of assistance in the fabrication of parts which were very important to my research, and Ms. Mie Sugimoto and Ms. Masako Morishita, the secretaries who were so kind and always supportive to me. Besides, it was so kind of the fellow student members in the laboratory for staying with me.

At the time when this thesis is edited, Hong Kong, which is my home town, is in a difficult time. Worried about the situation in my home town, I was dispirited in some moments. It was impossible for me to get through this tough time and complete the thesis without the supports from my best friends. So, I would like to express my deepest thanks to them. Also, I would like to thank my family for their love, support and patience.

Last, I believe that freedom of speech is of utmost importance to scholars. I would like to pay tribute to the Hong Kong people who have make an effort in the fight for freedom and democracy.

Contents

List of Figures

List of Tables

Chapter 1 Introduction

"Don't get set into one form, adapt it and build your own, and let it grow, be like water. Empty your mind, be formless, shapeless - like water. Now you put water in a cup, it becomes the cup; you put water into a bottle it becomes the bottle; you put it in a teapot it becomes the teapot. Now water can flow or it can crash. Be water, my friend."

- Bruce Lee, martial artist and actor (1940 - 1973)

1.1 Background

1.1.1 Modular robots

As reflected from many science fictions [1–4], human long have a desire to build structures which can be freely shaped on demand in a timely manner. The process of reconfiguring a structure involves breaking the structure into modules and configuring the modules into a structure of different shape, which implies the need for modularizing the elements of a structure, and driving modules into motions.

The concept of modular robot was originated from the Dynamically Reconfigurable Robotic System (DRRS) proposed in a previous study [5]. Unlike conventional robots which cannot be automatically reorganized by replacing links with others or reforming shapes to adapt to the working environments, the idea is to apply a cell system of living creatures to a robotic system, and to compose a robot by using several types of cells, including joint cells, adjustable cells, work cells, etc. The robot consists of these cells can detach itself and combine autonomously to construct robots of optimal configurations, such that it can adapt to restricted working environments, like a tank with small entrance, as illustrated in Fig. 1.1.

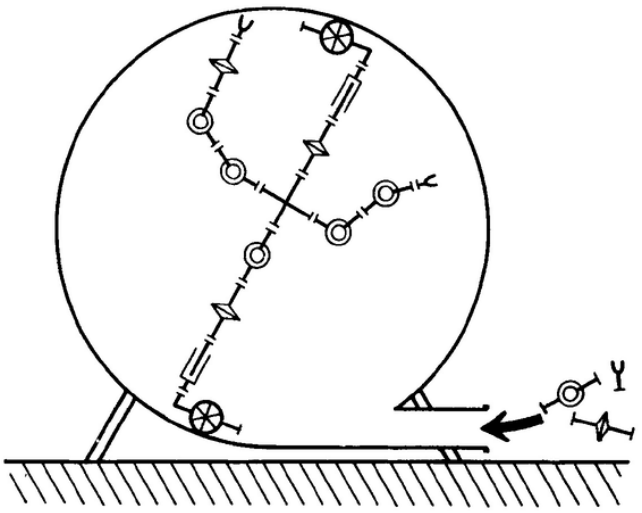

Fig. 1.1: An example of application of the DRRS for maintenance works in a storage tank [5].

In pursuit of this goal, many studies on modular robot systems (also known as "reconfigurable robots") have been conducted in the past two decades [6]. Equipped with bonding mechanisms, the modular robots developed in these studies are capable of forming linkage with the others. The resultant structures that can be constructed by modular robots can generally be classified into chain [7, 8] and lattice systems [9, 10]. In many cases, a joint and an actuator are included in a modular robot, and when these modular robots bond with the others forming linkages, locomotion can be resulted by moving the linkages using actuators. To allow effective locomotion to be performed with the structure formed by these modular robots, the maximum size of the structure has to be restricted, as the number of module that can be manipulated by an actuator is limited by it's maximum torque [7].

A breakthrough in this area is the development of M-block [11]. As a kind of modular robot, an important feature of M-block is the cube-shaped body with magnets installed on all faces, which allows robots to bond with other robots and form closely packed structure of different 3D shapes. The appearance of M-block is as shown in Fig. 1.2.

To support locomotion of the robot with no robot arm, M-block equips with an internal flywheel for actuation; by applying an abrupt brake on the fast rotating flywheel, a moment can be generated, which provides a torque for the robot to roll on the ground, and jumping motions can be observed when an instantaneous high torque is produced. This type of robot, which can be classified as a Mass-manipulated Rolling Robot (MRR), have an advantage that the internal struc-

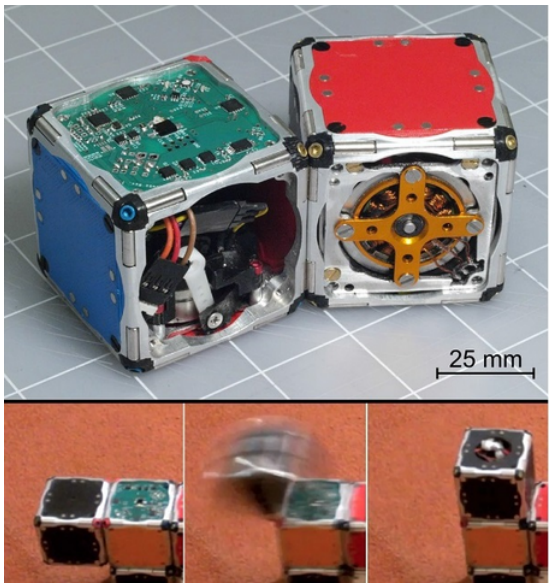

Fig. 1.2: The modular robots, M-blocks [11].

ture of the robot is completely isolated from the external environment, and therefore useful for locomotion in dusty environment [12].

However, because of having only one actuator in a fixed orientation, these robots can rotate in only one direction. Based on this configuration, the actuator of a module may occasionally be unaligned with the goal orientation for performing targeted motion, rendering the inevitability of using high torque for the reorientation of the module in a stochastic manner. This makes difficulty in proper control of a group of robot when performing task.

1.1.2 Rovers and structures in space

With the advance in aeronautics, space exploration has became a popular research topic [13,14]. For missions to be performed on plantery surfaces, rovers are commonly used, while rovers that use friction-based method for locomotion, like the wheel-driven Curiosity Rover [15], may not be desirable for exploration tasks on some small asteroid with microgravity [16]. Targeted at these environments with micro gravity, hopping rovers have been proposed in many studies [16–18]. Amongst these rovers, the use of snap-through-buckling mechanisms have been proposed as a simple and effective means of actuation [19,20]. Examples of rovers equipped with snap-through-buckling mechanisms include MINERVA-II and HORUS, as shown in Fig. 1.3 and Fig. 1.4 respectively. By applying the mechanism to MRR-type modular robots, it is expected that modular robot

can also be used on asteroids with microgravity.

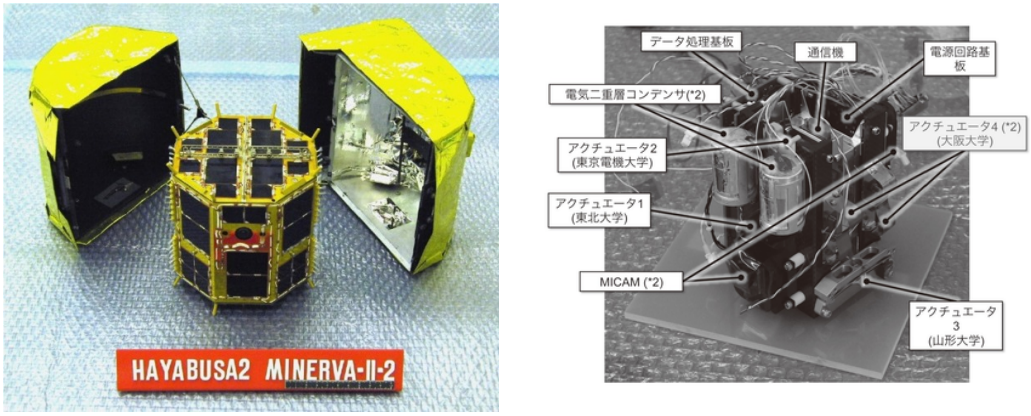

Fig. 1.3: The small asteroid exploration rover MINERVA-II [21, 22].

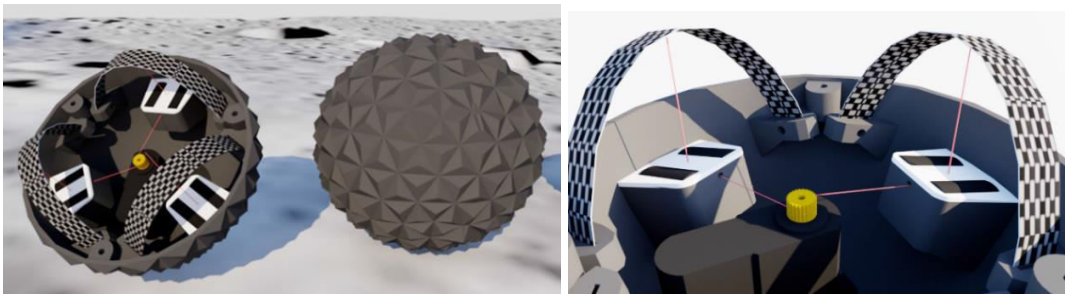

Fig. 1.4: The small asteroid surface rover HORUS [20].

Because the cost for replacement of malfunctioned robots in space is unquestionably high, collective systems, which have high robustness to failure of an individual, have been widely applied in space missions including planet exploration [23].

Related to space technology in recent years, there are studies aimed to support human live in space [24], which include space architecture [25]. However, as the capabilities of launchers are so limited even with the latest technology, transportation of large structures from earth to space remains as the biggest problem. Solution like collapsible or deployable structures has been proposed as solutions to overcome this problem [26–28], but most of these designs can only support structures of a particular shape, and none of these structures can generated any movement. An example of deployable structures is as shown in Fig. 1.5.

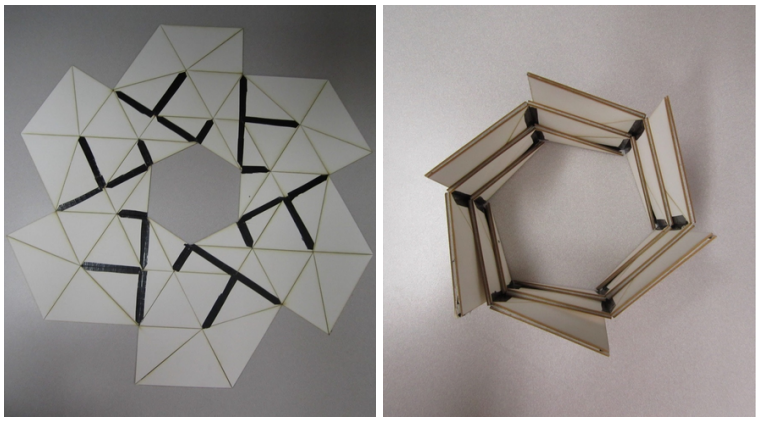

Fig. 1.5: An origami-based deployable array [28].

1.1.3 Multi-master communication between modular robots

For the control of collective systems, which include multiple agents, exchange of information is essential for reaching consensus amongst agents, especially when it is necessary to facilitate synchronization amongst agents.

The control of multi-agent systems can be generally classified into centralized and decentralized control schemes [29]. Centralized control is a commonly used method for the control of multiple agents, but has limitations due to escalated amount of data transmission with increased number of agents, and also the attenuation in signal strength caused by obstacles or other agents [30]. Amongst a variety of commonly used communication architectures, master-slave architectures can be useful for centralized control, but do not work well with decentralized control because there is no central leaders. Alternatively, a multi-master architecture can be effective for the communication between agents. As a popular communication protocol with a multi-master architecture, Controller area network (CAN) was developed by BOSCH as a multi-master, message broadcasting system [31]. As CAN is event-driven, bitwise-arbitrated and non-destructive, it is effective for broadcasting message in wired network. CAN has been applied in modular robot systems [32] [33], while wired networks are necessary in these robot systems.

For wireless communication in multi-agent systems, radio signal is commonly used [34] [35] [36], including the example as shown in Fig. 1.6, but the implementation becomes bulky and expensive when localization has to be supported in addition to communication [37]. For this reason, infrared(IR), which is an alternative solution for both communication and localization, is

widely utilized in multi-agent systems [38] [39].

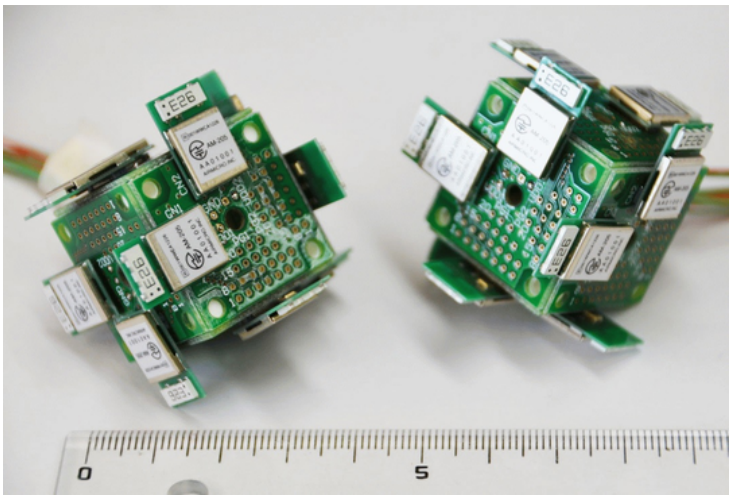

Fig. 1.6: Rovers equipped with twelve antennas for radio communication [34].

In order to implement CAN networks on mobile systems, wireless application of CAN by using IR for signal transmission has been proposed [40]. Because only 2 wire buses were required for the whole CAN network with variable number of nodes, wireless transmission of signal can be achieved by simply converting CAN signal to a single channel of IR light, which is relatively easy to be implemented when compared to other communication protocols. On the other hand, since one-way transmission of signal has to be kept between any 2 nodes, a chain or a tree formation is needed when repeaters were applied. This highly limits it's application on mobile distributed systems.

Similar communication with multi-master architecture can also be found in the nature, where flashing of fireflies can be synchronized without any leader or any formation for the fireflies to follow [41]. The key to syncrhonized flashing of fireflies lies in the predefined period of flashing, where signal from neighbors only affects the timing of flash but not the period. In comparison, the correction of the timing of flash in fireflies is similar to the adjustment in bit timing of CAN messages [42]. So, it is expected that by adding a mechanism on the repeater for forcing output signal to follow the default cycle of CAN communiation, communicaiton between distributed systems can be performed regardless of the formation.

1.2 Objectives

Being locomotive, robust to failure of an individual, capable of forming structures of various shape, modular robots are definitely ideal for space missions including space exploration and structure building. Furthermore, as the structures composed of these modular robots with build-in actuators equipped can also achieve locomotion, it may be possible to form movable structures, which can be a building or a bridge. Besides, by using the modular robots to surround existing objects of various size and shape, objects can attain higher stability to against overturn, hence the use of force generated by the robots surrounding an object can provide a reliable solution for object transportation. An absolute advantage of this method over traditional ways of object transportation is that the modular robot system is highly scalable, which allow objects of different size to be handled. So, it can be envisioned that the modular robots with such functionality can be applied in a wide range of fields.

Nevertheless, before achieving the ultimate goal of creating locomotive structures of various shape, and transporting objects in various size and shape, countless problems have to be addressed. In particular, the deprivation in freedom of movement of existing modular robots for effective assembling, the inadequacy in the efficiency of existing communication methods for supporting an effective decentralized control of distributed systems, and the lack of simple algorithm for the formation of structures with modular robots.

This study was conducted in order to address these problems. The study was started with the development of a modular robot for achieving high freedom of movement. Then, a multi-master communication platform was developed for distributed systems. Finally, by making assumption that a new modular robot can be produced, and with a simple control algorithm, a computer simulation was conducted to investigate the possibility of the formation of a locomotive structure by a group of modular robots in micro gravity environment.

1.3 Dissertation overview

Overview of this thesis is as described below.

In chapter 2, a novel design of the cubic robot Macrotis is discussed. The structure and the

action of the snap-through-buckling mechanism, and the installation of mechanical and electronic parts including the snap-through-buckling mechanism on the robot for supporting rolling and jumping motions in mulitple directions, are to be explained in detail. Experiments for investigating robot's motion under pseudo micro gravity environment are conducted, and results on rolling and jumping actions are obtained, which help verifying the capabilities of the robot.

In chapter 3, a design of multi-master communication platform is presented. Test modules equipped with the platform are constructed, where the mechanical structure of the module, the circuit and the relationship between input and output, are clarified. After introducing test software and rules on identifier for the prioritization of message, experiments on synchronization between modules in various formations are conducted by using the communication platform, which helps evaluating the performance of the platform in establishing effective communication between distributed systems.

In chapter 4, a new modular robot composed of the actuator part of Macrotis and the body frame of M-block is considered, which should theoretically support rolling and jumping motions in multiple directions, and bonding of robots. With information available to robots limited to distance between robots and the direction of gravity, rules are defined for controlling robots' action, so as to encourage formation of structures by robots. By using mathematical expressions, it is proved that a robot can approach another robot by rolling action according to the rules. A computer simulation is conducted to show that structures can be formed under this setting. To improve the credibility of the simulation, acceleration of mass in the snap-through-buckling action is analyzed by capturing video under high speed camera, and the parameterized result is added to the simulation model. With the force and torque acting on magnets corresponding to their positions and orientation in the field worked out per time step, 4 cases of simulation are performed with varying number of robots in the field. The effectiveness of the method on the formation of planar structures is reviewed with the statistical results obtained.

In chapter 5, all chapters are summarized, including the results obtained from chapter 2 to 4, and a conclusion is drawn on the overall result. By reviewing the overall results, areas that require further study in the future in order to fully satisfy the objectives are to be discussed.

Chapter 2 The cubic robot Macrotis

In this chapter, a new design of cubic robot is to be discussed, which can achieve rolling and jumping in multiple directions under micro gravity environment. The snap-through-buckling mechanism equipped in the robot as actuator, and the structure of the robot are to be explained. Through experiments under pseudo micro gravity environment, the performance of the robot on rolling and jumping was assessed.

2.1 Snap-through-buckling mechanism

Spring-mass systems can be used to generate translational force and are commonly used in inertia-driven actuations. Apart from complicated traditional designs of spring-mass systems with the use of helical compression springs, previous studies have found that high acceleration of mass can be generated by the snap-through-buckling action of a closed elastic strip [43]. This provides a good alternative in designing a spring-mass system. The snap-through-buckling phenomenon is illustrated in Fig. 2.1.

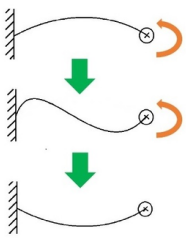

Fig. 2.1: Snap-through-buckling phenomenon.

In this study, a snap-through-buckling mechanism was developed that uses closed elastic strips to generate a translational force. The snap-through-buckling mechanism consists of a piece of elastic material that is made of thin metal strips and that has its two ends fixed to shafts. With the distance between the two shafts shorter than its length, the elastic material bends into an arc at a stable state. In current design, one of the two shafts (hereinafter referred to as "drive shaft"), is rotated while the other remains passive. When the drive shaft is rotated, the elastic material is deformed and energy is stored. This corresponds to the transition between the first two states in Fig. 2.1. At a certain angle of bending, snap-through-buckling is triggered and energy is released, as in the transition between the last two states in Fig. 2.1). Finally, the elastic material bends into an arc on the opposite side, entering another stable state. By using this mechanism, snap-through-buckling can be triggered consecutively. Also, by attaching a mass to the elastic material, a translational force can be generated and a translation motion can be induced. The structural design of the snap-through-buckling mechanism is shown in Fig. 2.2.

The advantages of using the snap-through-buckling mechanism are that it yields high acceleration, requires no return of spring, and results in less vibration on the system.

2.2 Robot design

2.2.1 Mechanical design

To allow the formation of closely packed structures, a cube-shaped body design like that for M-block is to be applied to the robot. Magnets are not to be included as the main purpose of this study is to demonstrate the high freedom of movement of the robot with the proposed design. To facilitate both translational and rotational motion with the robot, the degrees of freedom have to be increased so that all orientations are handled. The structual design of the robot is illustrated in Fig. 2.2.

Steps for installation are marked in the figure. In steps 1 and 2, two platforms with snap-through-buckling mechanisms were installed on the top and bottom faces of a cube (hereinafter referred to as the "inner body"). As both platforms are rotatable, a translational force can be generated when the two mechanisms generate forces at the same time in the same direction; a moment around the center of the inner body can be generated when those forces are in the opposite directions. In step 3, the inner body is installed into a larger, cubic outer frame. In step 4, a

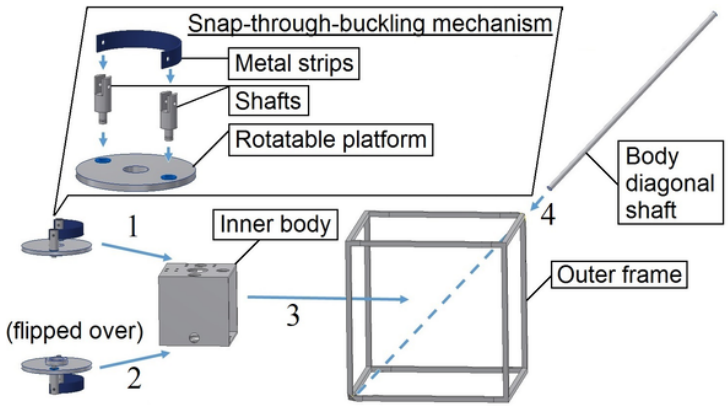

Fig. 2.2: Structural design of snap-through buckling mechanism and the robot.

shaft intersecting the body diagonal of both bodies (hereinafter referred to as the "body diagonal shaft"), is installed, such that the inner body can rotate around the body diagonal of the outer frame. The rotation of the inner body around the body diagonal shaft is shown in Fig. 2.3. In this configuration, the two platforms can be aligned with the horizontal level, regardless of the orientation when the outer frame is positioned horizontally on ground. This allows the robot to roll on ground. Similarly, translational force can be generated in multiple directions by adjusting the orientation of the inner body and the angles of platforms, and this allows the robot to jump.

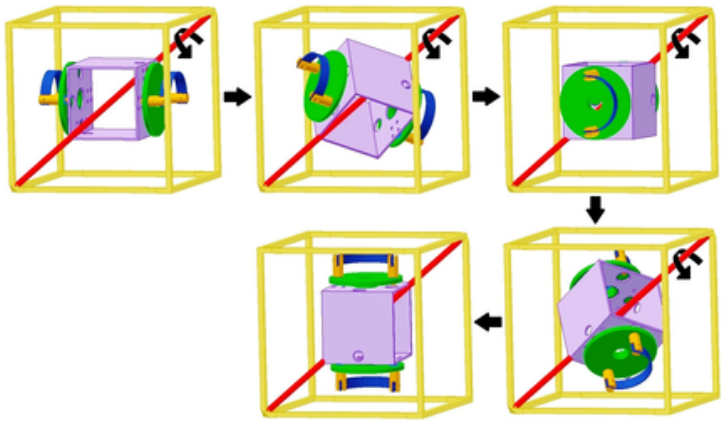

Fig. 2.3: Rotation of the inner body around the body diagonal shaft.

For the inner body to rotate inside the outer frame, the minimum size of the outer frame must be bigger than the size of the inner body. At the same time, a larger moment of inertia on rolling easily results when the size of outer frame is increased. It is therefore necessary to minimize the size of the inner body for the ease of movement.

The robot is shown in Fig. 2.4.

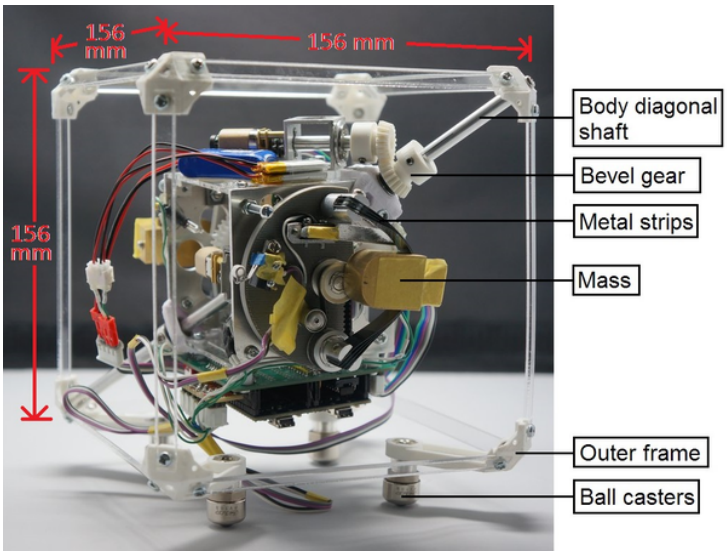

Fig. 2.4: Appearance of the robot.

It is worth mentioning the design of the snap-through-buckling mechanism, which provides adequate force to support the robot's movement. Because of limitations on the size of the inner body, the length and width of the piece of elastic material to be fixed on two rotatable joints are also limited. To find a suitable elastic material, experiments were performed with metal strips of different thickness, and it was found that there is insufficient output power when a single thin metal strip is used, while a thick metal strip breaks in two on bending. To overcome this problem, four thin metal strips were applied in the snap-through buckling mechanism, with spacers between each strip to reduce friction. Because the center points of the metal strips move along different paths when the drive shaft rotates, fixing the center point of all strips causes them to be severely deformed on bending, which is undesirable. Taking this into consideration, a hole at the center of one metal strip and slots on the others were made for attaching the mass. The metal strips for the snap-though-buckling mechanisms are shown in Fig. 2.5, where shafts and mass are installed by putting screws through holes and slots on the metal strips. The mechanism with metal strips installed can be seen in Fig. 2.4.

For one platform with a snap-through-buckling mechanism installed on the inner body, it is obvious that two motors are needed to turn the drive shaft and the platform, so four motors for two platforms are needed in total. By implementing two coaxial systems in the current design, all

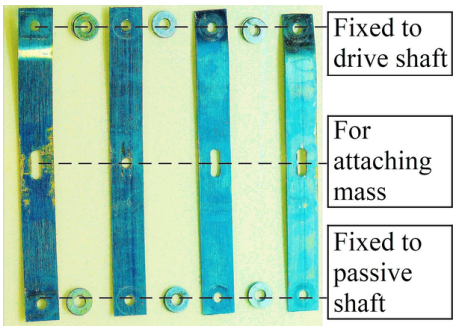

Fig. 2.5: Metal strips for snap-through-buckling mechanisms.

platforms and drive shafts can be driven by the motors installed inside the inner body. This helps to make the platforms compact and light. The configuration of the coaxial system is illustrated in Fig. 2.6. In this configuration, two actions can be performed by

1. keeping motor 1 stationary and powering on motor 2, and
2. turning motors 1 and 2 in the same direction at the same speed.

For 1 above, shaft C, and drive shaft A, which is connected to shaft C through a timing belt, are driven into rotation. This causes deformation of the metal strips mounted across drive shaft A and passive shaft B, and the snap-through-buckling of metal strips can be triggered as a result. For 2 above, shaft C and shaft D are driven synchronously. This causes a rotation of the platform that is connected to shaft D, while the snap-through bucking mechanism remains untriggered.

Besides of the four motors needed to turn the drive shafts and platforms, one extra motor is needed to turn the inner body around the body diagonal shaft of the outer frame. This motor is mounted on a face of the inner body in the current design. In order to allow torque transmission between the motor and the body diagonal shaft, the motor is aligned with the diagonal of the face, such that it is pointing at the body diagonal shaft with two axes intersecting at an angle of 35.2 degrees. By using bevel gears with corresponding shaft angles, torque can be transmitted between the motor and body diagonal shaft.

In current design, the robot weighs around 729g and each mass attached to the two snap-through-buckling mechanisms is 73g. The frame is mainly made of acrylic bars and PLA plastic to reduce weight.

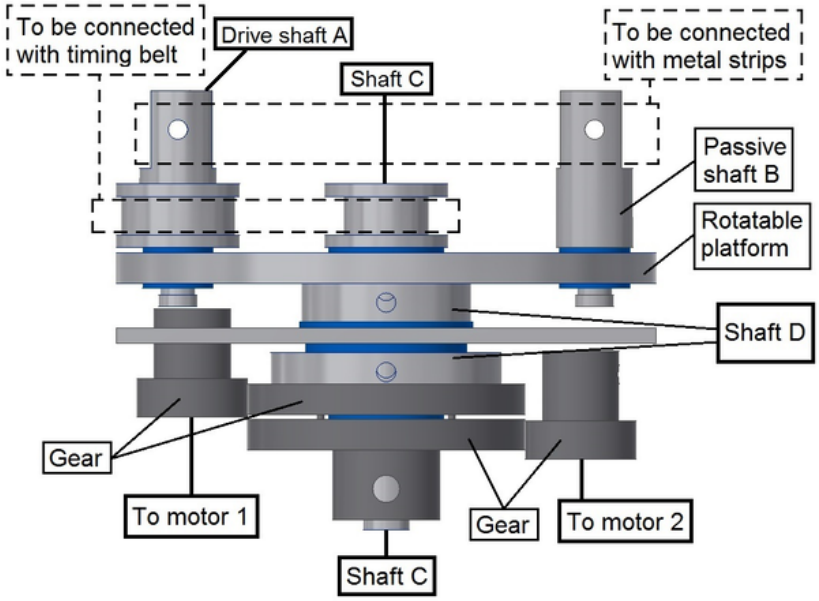

Fig. 2.6: Configuration of coaxial system.

2.2.2 Electronics and software design

Sensory devices, including incremental encoders, microswitches and mercury switches, are utilized for controlling robot's movement. As metal strips and platforms are driven by motors, their positions can be monitored by reading encoder signals from the motors after initialization by using microswitches.

For the generation of force in the target direction, it is necessary to detect the orientation of the robot. Advanced sensory devices can be applied, but just a few mercury switches are utilized in the current design. The simplicity of sensory devices can enhance the robustness of the robot. The configuration and states of the four mercury switches at different robot orientation are shown in Fig.2.7 and Table 2.1 respectively. Note that in Table 2.1, the "open" and "close" states of mercury switches are represented by "0" and "1" respectively. In the first 6 cases, one face of the inner body is aligned with the horizontal ground; case 7 to 10 are transition states indicated by "None". When a transition state is detected, the inner body turns around the body diagonal shaft until the robot is in one of the first six cases.

To drive motors and read signals from sensory devices, the circuit board consists of motor driver ICs and two Mbed LPC1768 microcontroller boards [44], in a master-slave architecture.

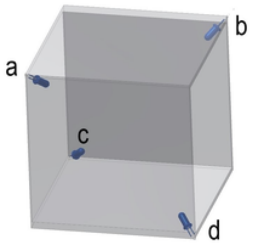

Fig. 2.7: Configuration of 4 mercury swtiches on inner body.

Table 2.1: States of mercury switches corresponding to different orientation of robot

Case	Face to the ground	State of mercury switches			
		a	b	c	d
1	Face with a & b	1	1	0	0
2	Face with c & d	0	0	1	1
3	Face with a & c	1	0	1	0
4	Face with b & d	0	1	0	1
5	Face with a & d	1	0	0	1
6	Face with b & c	0	1	1	0
7	None (between cases 1 & 3, 1 & 6, or 3 & 6)	1	1	1	0
8	None (between cases 1 & 4, 1 & 5, or 4 & 5)	1	1	0	1
9	None (between cases 2 & 4, 2 & 6, or 4 & 6)	0	1	1	1
10	None (between cases 2 & 3, 2 & 5, or 3 & 5)	1	0	1	1

All electronic devices are powered by two 3.7V, 110mAh and one 7.4V, 180mAh LiPo batteries.

In the program for embedded systems, encoder counts were read, and outputs to motors for driving platforms and drive shafts were determined by a simple P-control law in slave, where the targeted positions are given by the master.

2.3 Motion under micro gravity environment

To demonstrate the robot's motion under a micro gravity environment, experiment was performed on a slope, where the force component directed parallel to the surface of the slope acted as

the pseudo micro gravitational force. Frictional force that could affect the results was minimized by adding ball casters to the base of robot, and covering the slope with a thick sheet of glass. For a 1.5 degree inclined slope, the pseudo gravity is 0.026G, where G is the gravitational force on earth. The experimental setup is shown in Fig. 2.8. As shown in the figure, a concrete block was positioned on the sheet of glass, which acted as the virtual ground. Note that the angle of the slope (as indicated by θ) shown in the picture is different from that applied in the experiment.

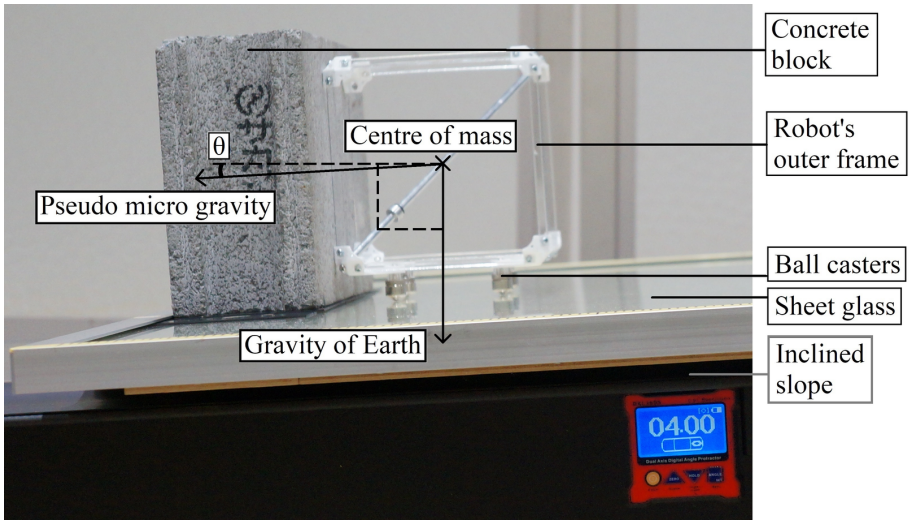

Fig. 2.8: Experimental setup.

In the original design, the robot could not roll along the slope because it automatically aligned the platforms to top and bottom sides before rolling. In order to perform experiment on the slope, the program was modified to make the robot align the two platforms horizontally. Noted that the small angle between surface of the slope and the ground was neglected in the experiment.

The rolling motion of the robot along the slope in the experiment is shown in Fig. 2.9. Note that the robot actually slides on the slope in the experiment, while all pictures in Fig. 2.9 were rotated 90 degrees anticlockwise for better understanding.

By demonstrating that the robot can roll forward for 90 degrees, it can be considered that locomotion can be achieved by repeated rolling, where the direction of acceleration of masses, and hence forces, can be adjusted by turning the inner body and platforms after each step.

Besides rotational motions, translational motion in different directions can be achieved by adjusting the angles of the two platforms. In order to show the maximum reachable height of the

robot under environments with micro gravity, jumping of the robot up the slope was demonstrated. The jumping motion of the robot on the slope is shown in Fig. 2.10. In the figure, the pictures were taken from the top, and the direction of pseudo micro gravity was as indicated in the figure. In the analysis of the captured video, the maximum jumping height of the robot is found as 203.7mm.

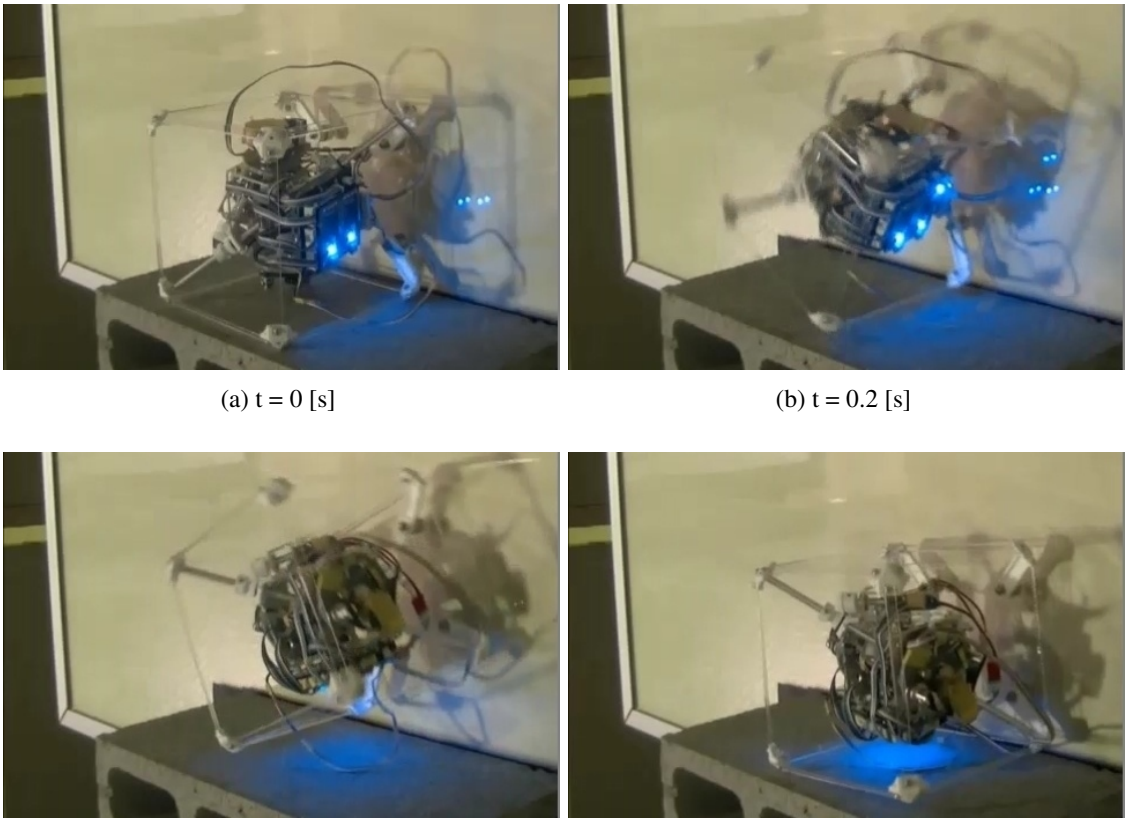

(a) t = 0 [s] (b) t = 0.2 [s]

(c) t = 0.4 [s] (d) t = 0.8 [s]

Fig. 2.9: Rolling motion of robot on slope.

2.4 Chapter concluding remarks

In this chapter, a new design of cubic robot using snap-through-buckling mechanisms as actuators was proposed. With electronic part and software included, the rolling and jumping action of the cubic robot was demonstrated under a pseudo micro-gravity environment.

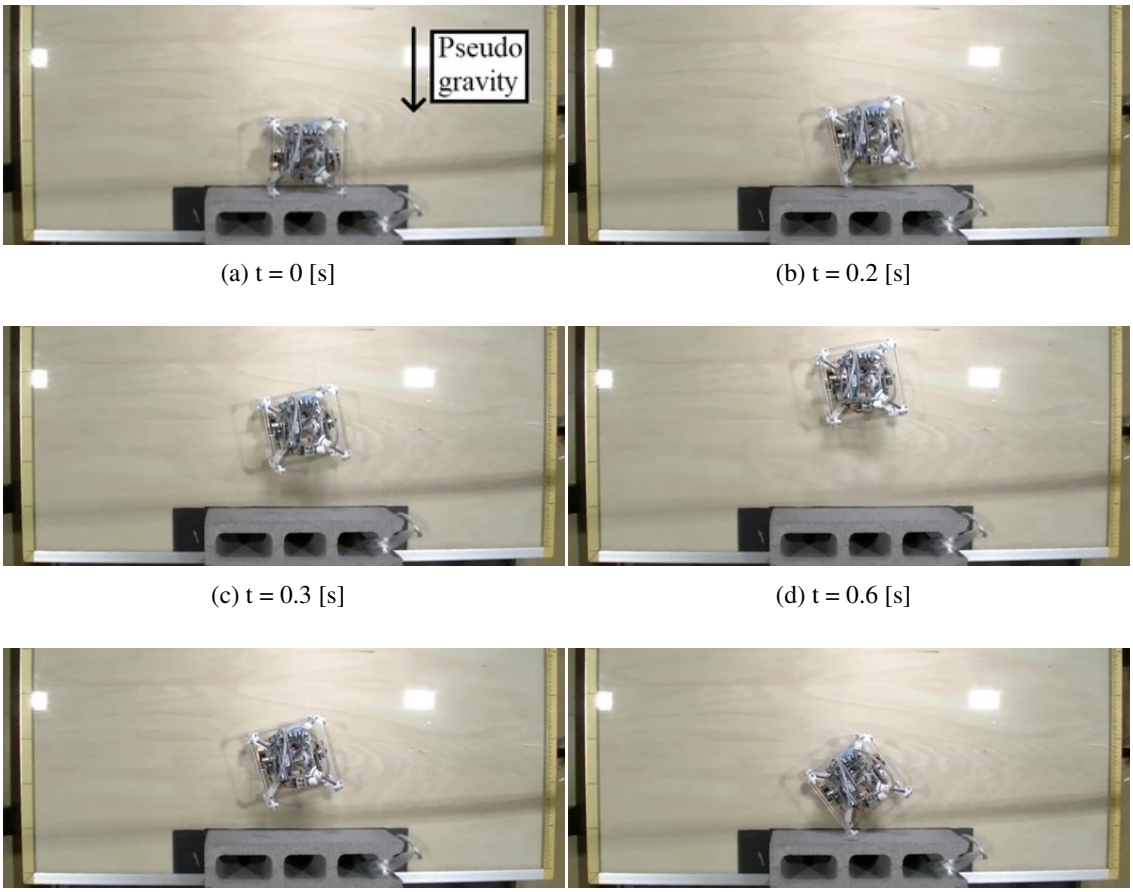

(a) t = 0 [s] (b) t = 0.2 [s]

(c) t = 0.3 [s] (d) t = 0.6 [s]

(e) t = 1.4 [s] (f) t = 1.8 [s]

Fig. 2.10: Jumping motion of robot on slope.

Chapter 3 Development of a wireless multi-master communication platform

In previous chapter, it is shown that a cubic robot with the proposed design can achieve translational and rotational motions in multiple directions. If the cubic robot can be expanded to a modular robot and assembled with the others in the same way as M-blocks do, locomotion of the resultant structure may be made possible by making use of the force generated by the individuals in collaboration.

Synchronization is necessary for performing such collaborated actions by robots, and a multi-master communication platform can be useful to the synchronization of distributed robot systems with decentralized control.

In this chapter, a wireless multi-master communication platform is proposed, which can be applied to distributed robot systems regardless of the formation. To verify the proposed system, experiments were conducted with test modules with the platform included, and the results show that synchronization of test modules can be effectively achieved with the platform.

3.1 Design of test module

3.1.1 Structural design

The produced test module is as shown in Fig. 3.1.

The cube-shaped design of the test module allows multiple modules to be piled up and form

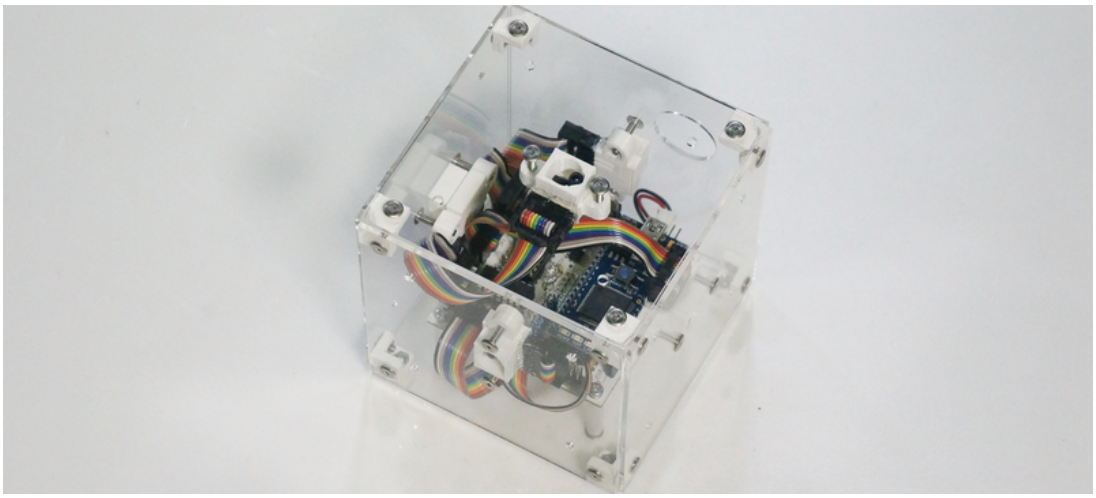

Fig. 3.1: Test module

different structures; the faces which are made of transparent arcylic sheets, allows IR light to pass through.

In each test module, IR transceivers (i.e. IR emitter and receiver pairs) were installed at all 6 faces with 1 pair at the centre of each face, via PLA plastic mountings produced by using 3D printer. This allows signal to be transmitted in all 6 directions, irrespective of the orientation of the test module. Similar to the configuration of antennas on a kind of exploration rovers [34], a mesh network can be established by test modules, which offers multiple redundant communication paths and hence having a high robustness against missing or failures of modules.

An electronic circuit board were installed into each test module for handling the input and output signals.

3.1.2 Electronic circuit design

Electronic system for CAN communication

In the electronic circuit, a microcontroller (MCU) with built-in CAN interface was used, with a CAN transceiver connected in-between, a local bus-line can be set up on the circuit board.

To facilitate wireless transmission of CAN signal, the local bus-line was connected to all IR emitters through drivers, such that IR light is emitted when there is a dominant bit on the bus-line. Also, to allow receival of CAN signal from the environment, input signals given by active-low IR sensors, which gives a low level output on detection of an IR signal, were merged by a NAND

gate and then added to the bus-line, such that the local bus-line is driven into dominant state when IR light is detected by any 1 or more of the IR sensors. Under this setting, the system acts as a repeater; CAN signal can be propagated at a short period of time over distributed systems as time delay in signal transmission is mainly caused by the hardware. The overall effect is the formation of a virtual bus-line in the air, with signal transmitted by IR lights.

The type of IR sensor chosen for the module gives a low voltage output when IR light with carrier frequency around 56 kHz is detected. Corresponding to the format required by IR sensors for signal detection, an intermediate output is first given by the driver according to CAN signal, which is then merged with a square wave of frequency around 56kHz, so as to produce pulse carriers for driving current through IR emitters. The square wave is generated by a PWM output provided by the MCU.

The bus is connected to an input pin of the MCU, such that PWM signal can be set on external interrupt events, and cleared according to the bit rate of signal transmission and the delay time of the IR sensors used. With adjustment on the duration of segments included in CAN bit time, good quality of signal transmission can be ensured.

To match the bandwidth of the IR sensor, a type of CAN transceiver that supports a low rate of data transmission was selected. In addition, each module is equiped with an LED for testing purpose.

Tackling deadlock loop with repeaters

When multiple repeaters are used in the same field, it is possible that the signal emitted by a repeater is propagated back to itself through the retransmittion of the same signal by 1 or more repeaters. A deadlock loop is formed as a result of this endless repetition of signal. The state diagram of a deadlocked system is as shown in Fig. 3.2.

While it is clear that this problem can be avoided by restricting the possible formation of distributed systems as described in previous work [40], looping of signal can be prevented with good design of electronic system used for communication. This can be achieved by introducing 2 rules into the electronic circuit. The 2 rules are as follows.

1. Input signal is only passed to all other output channels.
2. For all channels with output, input signals are ignored.

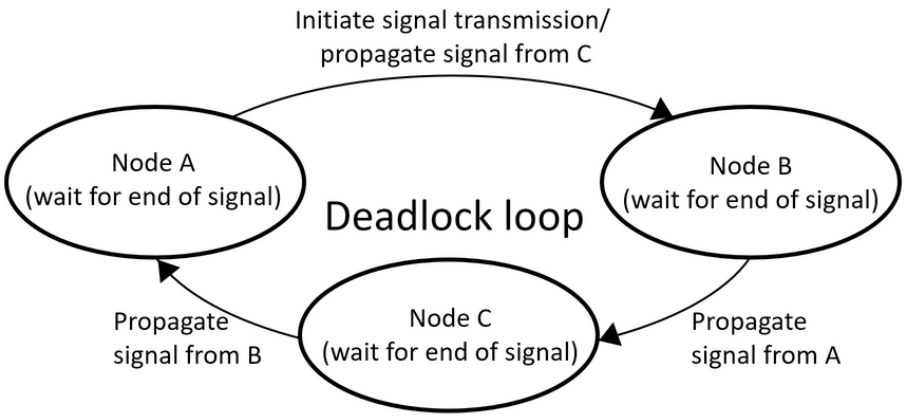

Fig. 3.2: The state diagram of a deadlocked system

These 2 rules can be implemented by adding AND and OR gates to the system. The block diagram for the system with deadlock prevention is as shown in Fig. 3.3, and the actions of logic gates are as shown in Table 3.1 and 3.2. Note that both tables are corresponding to the states of a single channel, while the output of OR gate in all other channels are assumed to be 1 and do not affect the result when the output of NAND gate is determined in Table 3.2.

Table 3.1: Driver's output with inputs coupled with an AND gate

Input from IR sensor	CAN Bus-line	Output of driver
0	0	0
0	1	0
1	0	0
1	1	1

In current design of test module, IR light is emitted and received at the same position for each channel. Under this setting, it can be assumed that if the IR light emitted from module A can be received by module B through certain channels of the 2 modules, module A can also receive IR light emitted from module B through the same pair of channel.

Based on the 2 rules introduced in the electronic circuit, transmission of signal can only be in 1 direction, where the direction depends on which of the modules first emits signal. It is obvious that the master module, which is the first to send signal to others, emits signal to all directions.

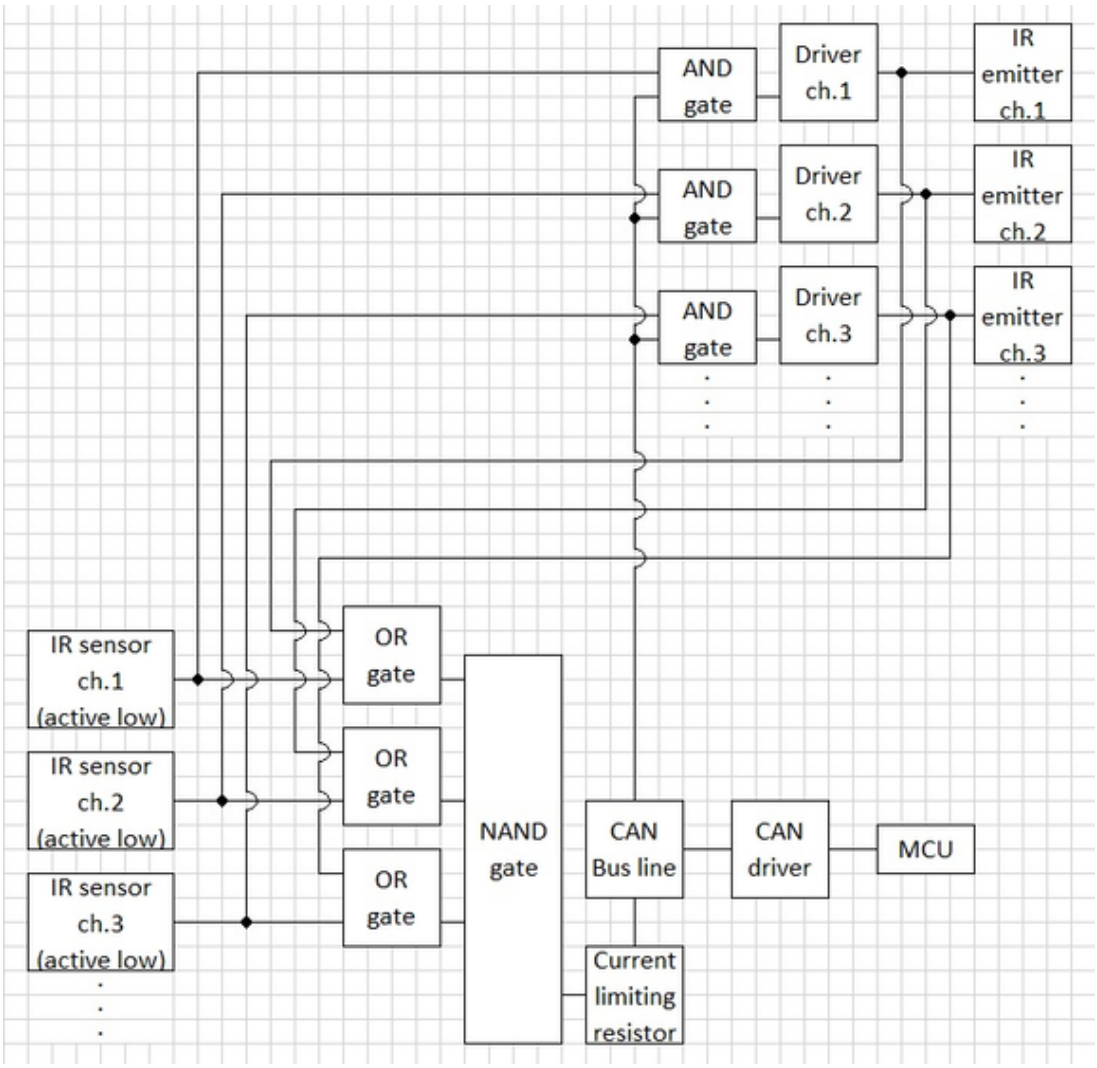

Fig. 3.3: Block diagram for electronic system with deadlock prevention

Table 3.2: Input to the CAN bus-line

Output of driver	Input from IR sensor	Output of OR gate	Output of NAND gate
0	0	0	1
0	1	1	0
1	0	1	0
1	1	1	0

For a rare case that signals are emitted at exactly the same time by a pair of channel of different modules, emitted signals are to be ignored by both of the channels. In this case, both modules

can operate normally without detection of signal emitted by another side because a dominant bit is already hold by both sides at the same time.

By taking modules as nodes, the communication established between them as edges directed from the sender to the receiver, the relationship between modules can be expressed in a graph. As the signal is sourced from the master to other modules, the overall system can be described as a graph with edges connected between nodes, directed from the master to all other modules.

With such a relationship between modules, signal from the master can only propagate outward but not going back, and hence no loop can be formed. This condition is true even when there is a large total delay of time for a signal to propagate across a number of modules, which can be accumulated by the time delay of IR sensors, IR diode and drivers included in each module.

The schematic of the electronic circuit board is as shown in Fig. 3.4.

In the circuit board, 6 connectors were included for connecting the board to 6 channels of IR emitter and IR sensor; IR emitters TSAL6200 were connected across pins labelled as “IR_OP” and “GND”, and IR sensors TSOP34156 were connected to pins labelled as “5V”, “GND” and “IR_IP”.

3.1.3 Software design

Testing on synchronization between modules

For testing on synchronization, the testing LED of modules are to be flashed periodically with their own timings. If the timings of the modules are synchronized, this should results synchronized flashing of LED.

To control the flashing of LED, the duty cycle is controlled by using 2 timer counters, i.e. on-count and off-count. When modules are powered on at different timing, LED in modules flash with their own timing before reaching any consensus with the others.

By establishing communication between modules, information such as off-count can be exchanged, which can help synchronization of timing for flashing LED on modules. It is straightforward that the effectiveness of the proposed platform can be proved by showing that synchronization of test modules can be achieved.

Because all test modules can send their off-count to the others during communication, it is

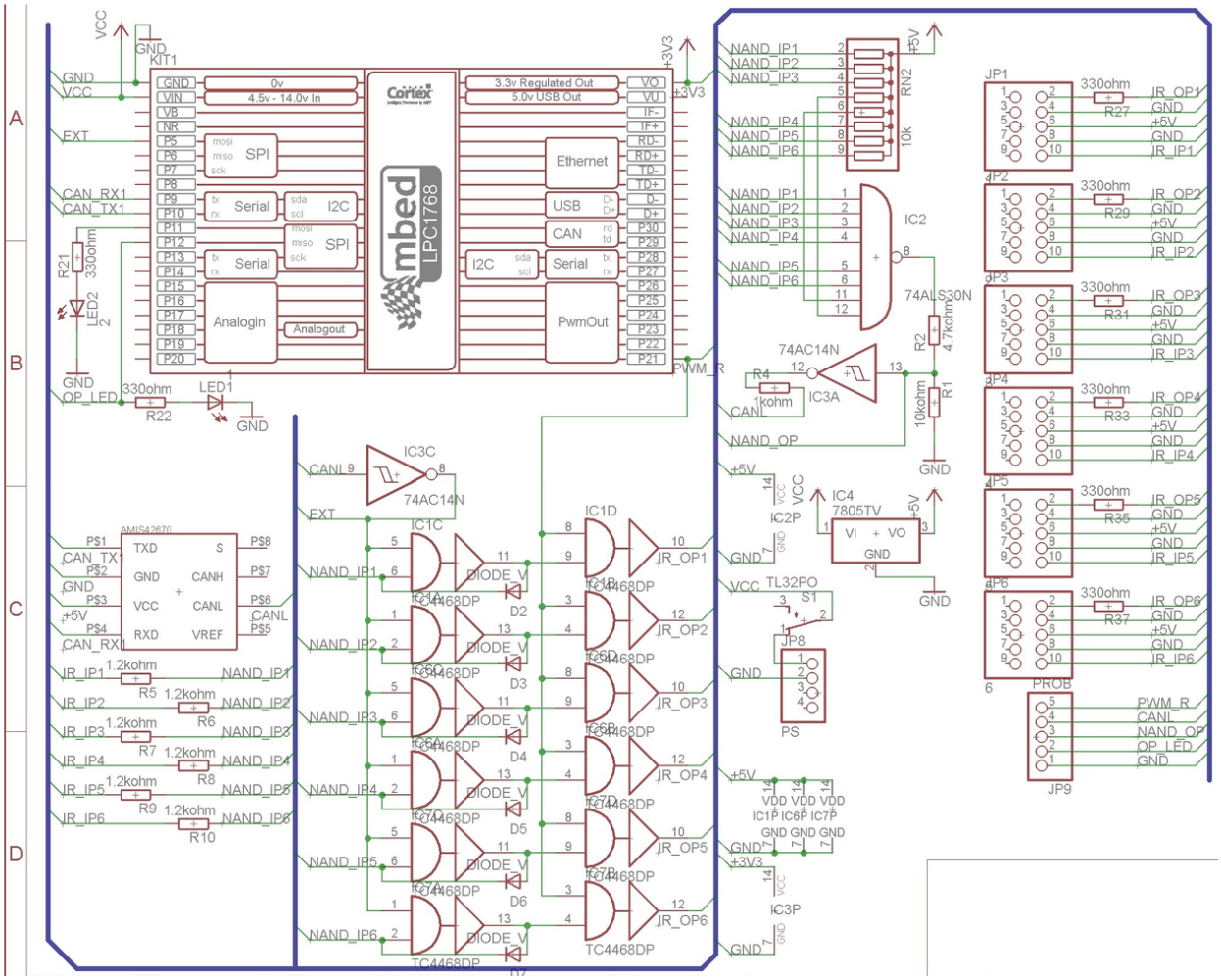

Fig. 3.4: Schematic of electronic circuit

necessary to establish a rule for determining which set of off-count is to be followed by all test modules. A solution for this is to assign priorities on the messages, which is similar to the method used in pherobots [45], where a hop count is included in the message for prioritization.

CAN bit timing configuration

By using mbed LPC1768 as the microcontroller and CAN transceiver AMIS-42670, CAN communication at a bit rate of 1200 Hz can be achieved. The communication rate for current test module is set as 4Hz.

Under current system's configuration, each pair of IR emitter and IR sensor were installed without any blockage between each other, and IR light emitted by an IR emitter can enter the IR

sensor in the same channel.

With the help of logic gates, detection of a dominant bit can be prevented at the moment while it is sent. However, a module may fall into deadlock loop after sending a dominant bit because IR sensors hold the logic for a long period of time after the IR signal is cleared. To avoid this problem, duration for holding the logic of a dominant bit has been adjusted so as to compensate the long time delay of IR sensors, where the logical high is cleared after the first 524μs until the end of the bit with a total duration of about 833μs.

To ensure that bits in CAN signal can be read at the best timing, the 2 phase segements for controlling the timing of bits were adjusted by modifying register LPC_CAN1 from the original setting of 0x4d43e7 to 0x7a43e7, where segements 1 and 2 in a bit, which is divided into 20 counts, were decreased and increased by 3 counts respectively. This results a shift in sample time, and each bit is read at 500μs from the start, which is in the logical-high region of a dominant bit.

Use of identifier for prioritization of message

According to CAN's standard, an identifier (ID) is included in every CAN message, which plays an important role to prevent collision if 2 or more CAN messages were sent by nodes simultaneously. This provides a good way for setting priorities on the messages sent by different modules.

First of all, assume that all CAN messages sent from any module can be received by all of the other modules. By offering a unique local ID to each module, modules can compare the value stored at their own IDs with that of the CAN messages received; CAN messages with a lower value are to be accepted, and otherwise rejected, by modules. Hence, CAN messages from different modules can be prioritized. On acceptance of a message, off-count in modules are to be adjusted. With difference in off-count between modules eliminated, synchronized flashing can be achieved. Because CAN messages with high value in ID have no significance over that with low value in ID under this setting, sending of message is to be disabled for a certain period when a message with a lower value in ID is received, and enabled otherwise. This helps to reduce the traffic of the bus.

Unfortunately, poor transmission of signal can occur in communication, especially when signal in the format of IR light is transmited in space with obstacles. To tackle the error in messages due to poor transmission of signal, procedures for error checking were included according to CAN's

standard, where messages failed to pass the checking were not to be accepted. So, it is fair to assume that under some circumstances, CAN messages sent from the module with the lowest ID (i.e. messages with the highest priority) cannot be delivered to all of the other modules. This potentially causes blocking in the propagation of message when a module with a high value in the ID is situated between modules with lower value in the ID, as sending of message is continuously disabled when a module keeps receiving messages with lower value in the ID.

To overcome this, the 11 bits ID field was modified by dividing into 3 parts, as shown in Table 3.3.

Table 3.3: Field allocation of 11 bits identifier field

Bit	10	9	8	7	6	5	4	3	2	1	0
Field	Delimiter			Master ID				Local ID			

With a 3 bits delimiter indicating the start of the ID field, corrupted messages can be easily filtered out with suitable ID filter applied. The master ID field is filled with the local ID of the module at the initial stage. On receival of CAN message, same ID-comparing rule was applied and the master ID field is to be overwritten by that in accepted messages. By doing so, modules can change the priority of their messages according to the message with the highest priority which they received. As a result, message from module with the lowest local ID can be propagated without any blocking.

A program was designed to achieve the objective of facilitating synchronized flash of all modules, and the operation of the program is to be explained. To begin with, in each module a timer counter called “led off count” is used to allow it to flash periodically. So, it is obvious that flash of modules can be synchronized by synchronizing the led off count in all modules. As the first step, all modules have to share their led off count to the others by broadcasting messages. To determine the set of led off count to be followed by all modules, the abovementioned priority scheme is applied, where an ID is also included in the message besides of led off count. By comparing the value of ID between messages and local, modules correct their led off count according to messages with lowest ID received, and discard the messages with higher ID.

Because messages with high ID have no significance, sending of message from a module is

disabled for a period, which is controlled by using a timer counter called “slave timeout count”, when a message with lower ID is received so as to reduce the traffic. The period is cleared when a message with higher ID is received. The flow of the program is as shown in Fig. 3.5.

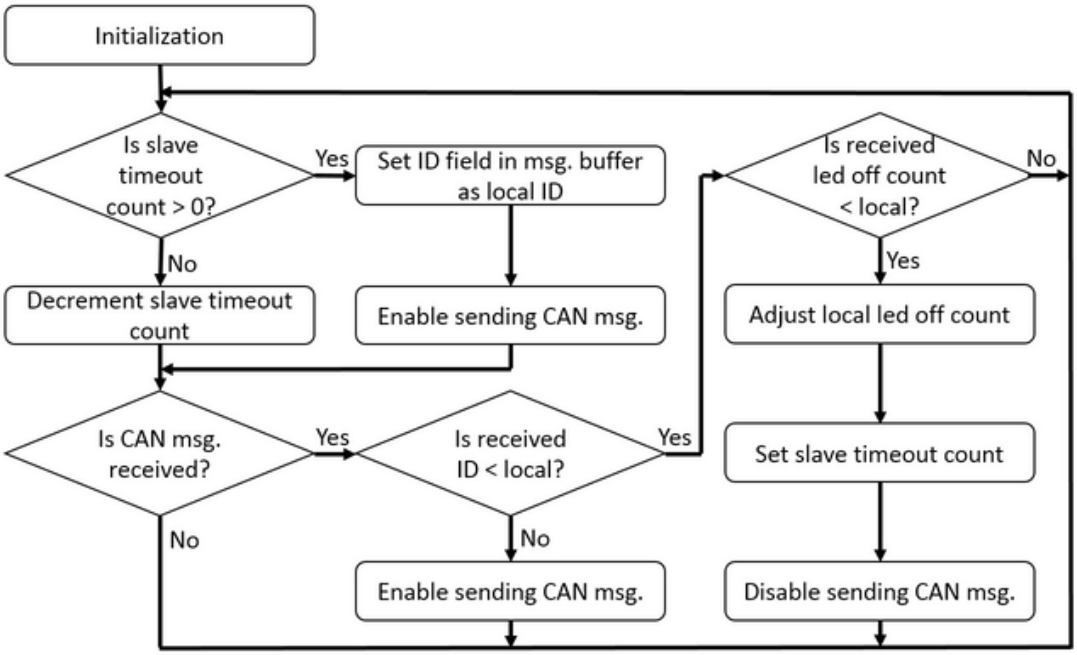

Fig. 3.5: Flow of the main program

3.2 Experiment with test modules

Through an experiment with 2 test modules, it is confirmed that communication can be performed between 2 modules at any angle, but with the range decreases with the difference in angle. The measured maximum distance for good communication is as shown in Table 3.4.

Table 3.4: Maximum distance for good communication

Angle of sending module (deg)	Max. distance (m)
0	10
45	2.9

In order to verifiy that communication can be established and synchronization can be achieved in all modules regardless of the formation, experiments were also performed with 8 modules positioned in 4 formations, which were line, ring, scatter and cube, as shown in Fig. 3.6. To allow easy observation of the timing of signals, test modules were started with a random number assigned to the off count, and with a random delay time within 16ms. Note that the cables attached to the test modules were only for issuing start signal and analyzing signal in test modules.

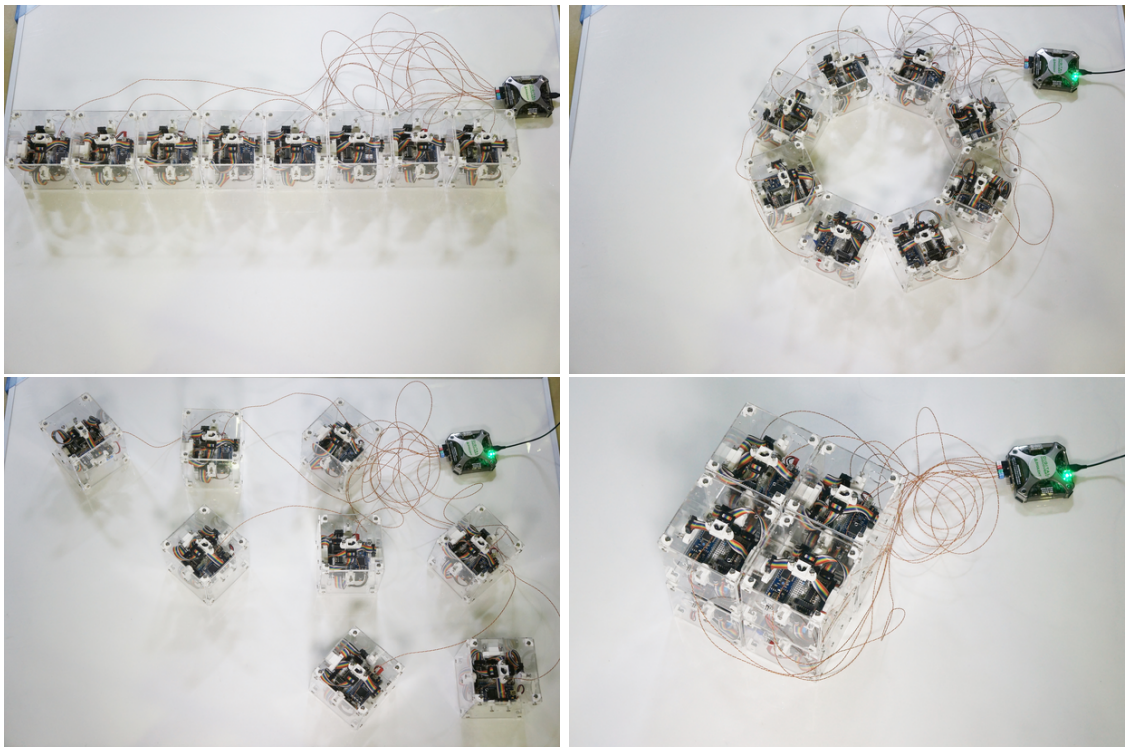

Fig. 3.6: Test modules in different formations: line, ring, scatter and cube.

In all experiments, it was observed that test modules flashed in different timing at the beginning but the differences in phase drastically decreased soon after start. Because there is no major differece between the signal-time graph for modules in different formations, only signal-time graph on modules in ring formation was focused in further analysis.

In order to compare the timing of signal with different number of test modules involved, the same experiment was repeated with 5 modules in ring formation, where the corresponding signal-time graph are as shown in Fig. 3.7 and Fig. 3.8 (enlarged view of highlighted region in Fig. 3.7).

As shown in Fig. 3.7, after starting, regular intervals can be observed because the duration for

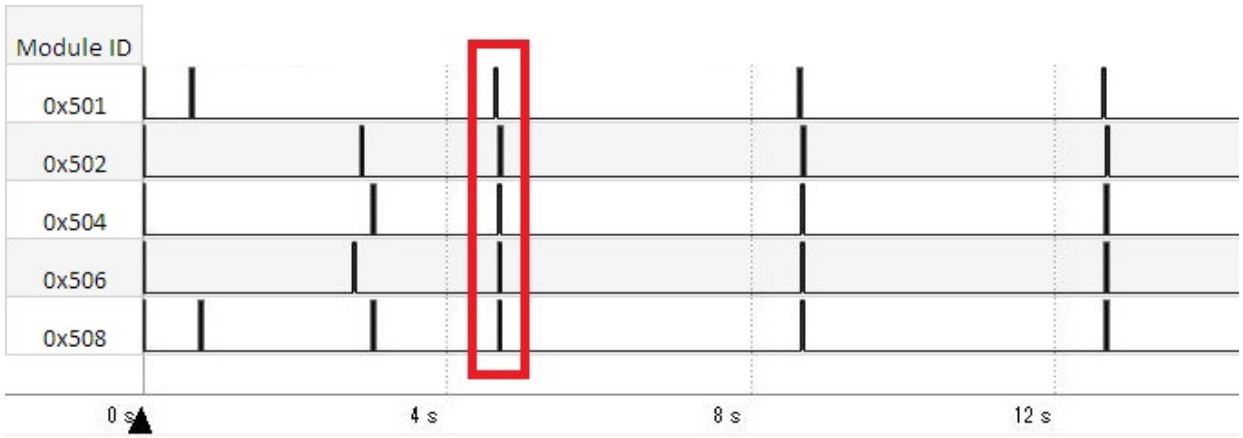

Fig. 3.7: Signal-time graph for LED flashing of 5 modules in ring formation

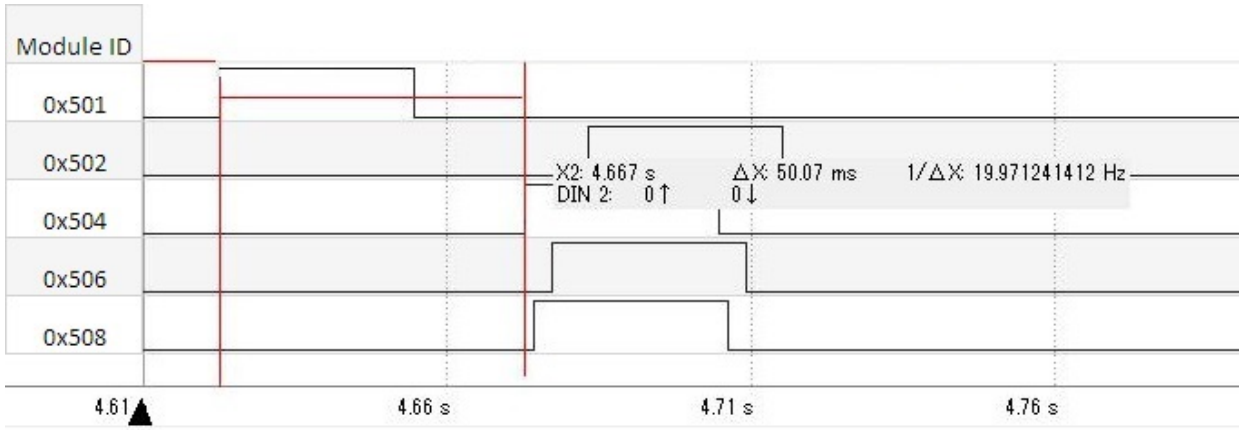

Fig. 3.8: Enlarged signal-time graph for LED flashing of 5 modules in ring formation, showing the highlighted region in the previous figure

turning the LED on and off were strictly controlled.

As channels were arranged with module's local ID in ascending order from top to bottom of the signal-time graph, it can be confirmed that intervals of flashing on modules with higher local ID were always corrected by that of the module with the lowest local ID that was available at the time. For simplicity, the module with the lowest local ID can be referred as the master, and the other modules can be referred as slaves. This matches the abovementioned identifier-comparing rule. In Fig. 3.7, it can be observed that synchronization was reached and all modules were flashing with almost the same phase at around 4.6s. Similar patterns were observed in all cases, with a lag on the signal of slaves following after that of the master, which is mainly due to the time required for transmitting a CAN message, and also the fact that difference in time within 1 off-count cannot

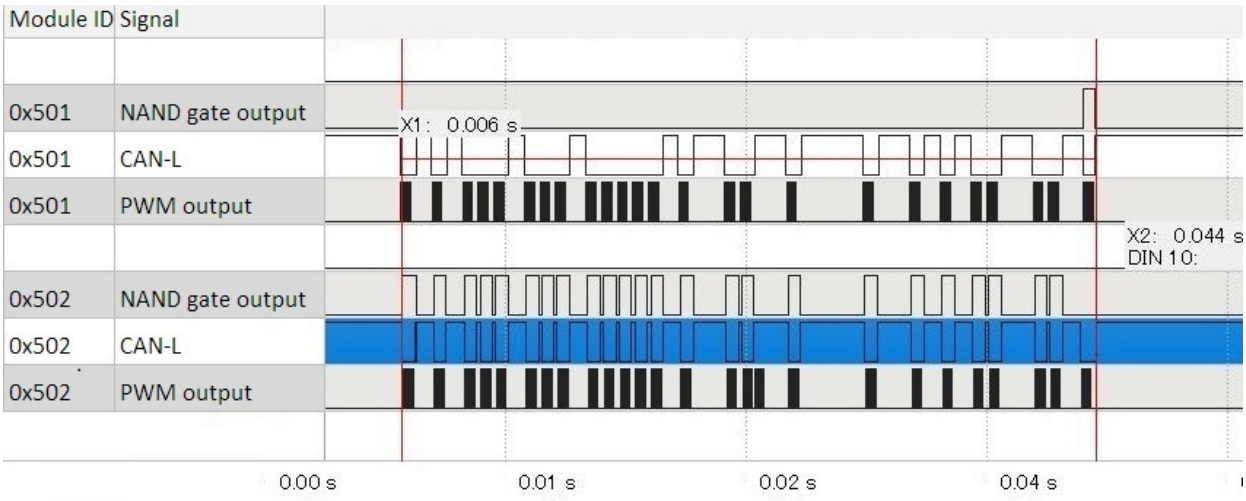

Fig. 3.9: Signal-time graph for a CAN message

be corrected, where 1 count is set as 16ms under current settings. As a reference, the signal-time graph for a CAN message is as shown in Fig. 3.9, and the duration of a CAN message is measured as 37ms (highlighted part). Note that actual duration of CAN messages can vary because of the bit-stuffing rule under CAN's standard.

3.2.1 Evaluation of performance

Experiment in ring formation was conducted 20 times on each of the cases with 5 and 8 modules. Because the maximum absolute time difference between the flashing of master and slave modules at steady state is found to be 218ms, it is taken as the criterion for synchronization, i.e. flashes are said to be synchronized when the time difference of signal between master and all slave modules are within 218ms. Statistics on the time duration from start to first synchronized flash for 5 and 8 modules cases are as shown in Table 3.5, and that on absolute time difference between master and slaves at first synchronized flash for 5 and 8 modules cases are as shown in Table 3.6. Note that 'S.D.' stands for standard deviation in both tables, and only the signal of slave modules are counted in all statistics.

In the result as shown in Table 3.5, it is found that first synchronization of flashing between modules ranged from 0.65s to 11.80s, and about 2.96s to 4.13s in average. Larger maximum value and standard deviation are observed in 8 modules case, for first synchronization of flashing. This is because of the potential increase in the communication delay when more modules

Table 3.5: Statistics on time duration from start to first synchronized flash (in ms) with 5 and 8 modules in ring formation

Number of modules	Min.	Max.	Average	S.D.
5	1022	7764	2960	1655
8	653	11800	4132	2462

Table 3.6: Statistic on the absolute time difference (in ms) between master and slaves at first synchronized flash with 5 and 8 modules in ring formation

Number of modules	Min.	Max.	Average	S.D.
5	11	207	69	42
8	1	218	66	43

are involved, where test modules compete with others for sending message along the bus before receiving message with higher priority. In the result as shown in Table 3.6, well synchronization between modules can be shown by the very small standard deviation of absolute time difference between master and slaves, which are 42ms and 43ms in the 2 cases.

3.3 Discussion

In the experiment, synchronization of test modules in 4 formations were demonstrated. This shows that communication can be successfully established between test modules regardless of the formation, and can be applied to distributed systems in random position. It is then natural to expect the application of the proposed platform on mobile distributed systems.

The goal of the experiment was to reach synchronization between test modules. To control the timing of flashing, messages sent by different test modules were set with different priority according to their randomly assigned local ID. This is because the goal can be reached by using 1 set of timing, and there is no preference on which set of timing has to be followed. It should be noted that the usage of the platform can be extended beyond the current aspect. For example, if robots are used in a task for searching an object and have to be assembled on discovery of an object, then the task can be performed effectively by letting robots to send message with high

priority on detection of the object. In other words, the identifier in CAN message can be very useful for prioritizing messages sent by distributed systems, so as to reach a consensus when performing various tasks. Besides of the standard 11-bit identifier used in the current system, extended CAN provides a 29-bit identifier which allows increased length for priority setting.

In the test module, a type of low cost IR sensor with relatively large delay was applied because speed of communication is not the focus of this study. While IR sensors with faster response time are available, it is possible to speed up the data rate. Besides, as signal is transmitted in the format of IR light, it can be expected that speed of communication can be further increased with suitable arrangement of optical fiber and optical amplifiers for spanning IR light emitted by 1 module over multiple modules.

3.4 Chapter concluding remarks

In this chapter, a wireless multi-master communication platform was proposed, which allows communication to be established between randomly positioned distributed systems. With the implementation of a priority scheme using the identifier, it can be shown that the proposed platform is effective for leading these distributed systems to synchronized action.

Chapter 4 Formation of locomotive structures in micro gravity environment

In chapter 2, the design of cubic robot which allows rolling and jumping motions in multiple directions to be performed was discussed. With such a design, it can be expected that an innovative modular robot can be created by combining the actuator mechanisms of Macrotis and the body of M-block, which adds bonding function to the robot. Besides, with the multi-master communication platform as discussed in chapter 3, actions of a group of robots can be highly synchronized, which makes locomotion of the resultant structure feasible.

In this chapter, a control algorithm for using this kind of new modular robot in the formation of planar structures under micro gravity environment is to be discussed, and the effectiveness of the algorithm was verified by the results obtained from computer simulations.

4.1 Design of new modular robot

The new cubic robot consists of the actuator part of Macrotis [46] for performing translational and rotational motions in multiple directions, and a body frame similar to that of M-blocks [11] for forming closely packed structures with robots. Readers can refer to chapter 2 for the details of Macrotis.

The possible directions for generating force and torque, according to the defined body coordinate of the robot which has the origin at the centroid, with x-, y- and z-axes perpendicular to faces at the front, right and top side of the outer frame respectively, are as shown in Fig. 4.1. It

is clear that the robot is capable of generating torque at centroid about all axes in both clockwise and anticlockwise directions, as indicated by τ_x, τ_y and τ_z in the figure; and also force from the centroid to any direction on planes including any two axes, as indicated by F_{xy}, F_{yz} and F_{zx} in Fig. 4.1.

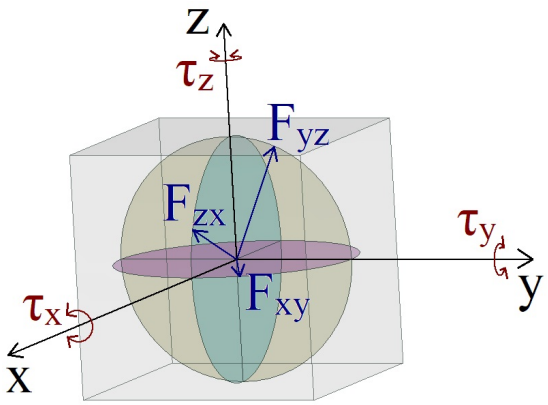

Fig. 4.1: Directions for force and torque output of the robot.

In other words, when the robot is placed horizontally, with the x- and y-axes of it's body coordinate parallel to the ground, which is just like the robot as shown in Fig. 4.1, the robot can generate a torque τ_x or τ_y for rolling, or a force F_{yz} or F_{zx} for jumping. Same rolling and jumping motions can be achieved when the robot is place on the ground in other orientations, as the orientation of the actuator inside the robot can be adjusted accordingly.

To facilitate bonding between robots, the design of the body frame of the robot is based on that of M-block, where twenty-four free-to-rotate diametrically polarized cylinderical magnets were situated coaxially with the edges of the frame, and eight disc magnets were arranged in an eight-way symmetric pattern on each of the six faces. The robot is as shown in Fig. 4.2.

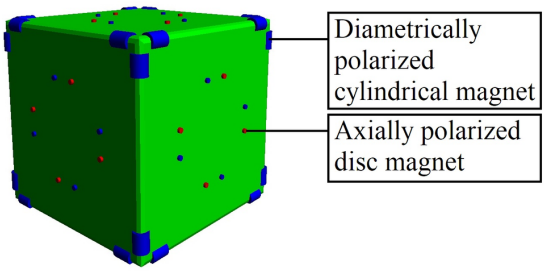

Fig. 4.2: The robot with modified configuration of magnets.

Seventy-two magnets were included on a robot in total. As shown in the previous study of M-blocks, this configuration allows magnetic bonds to be formed on edges, with disc magnets help aligning the robot during bonding. Minor modifications in the position of magnets have been made to the robot, so as to reduce the chance of misaligned bonding.

The robot is equipped with one sensor to detect the direction of gravity, and one distance sensor at the centre on each face, for measuring the distance between robots.

4.2 Rules for robot's action

To achieve the goal for forming a structure with robots, rules were set for controlling robots' action. For determining the action to be taken, robots make the best use of the direction of gravity, and the distance from other robots. For simplicity, the distance between the centres of two robots were used in calculation.

As a kind of mass-manipulated rolling robot (MRR) [47], rolling is an effective way for locomotion. However, a robot can no longer perform rolling effectively when it is coupled with the others, or when it is potentially obstructed by other robots. To handle such cases, jumping is performed by using snap-through-buckling mechanisms, which was demonstrated in previous studies [19] [20]. So, before taking any action, it is necessary for a robot to acquire the state of being coupled with the others or not. Given s as the side length of the cubic robot, two horizontally positioned robots are potentially in contact when the distance between them is less than or equal to $\sqrt{2}s$, which is equal to the length of face diagonal of the cubic robot, as illustrated in Fig. 4.3. So, a robot is considered as in "united" state when there is a robot situated at a distance d less than or equal to $\sqrt{2}s$ from it, and otherwise considered as in "isolated" state. The two states, and the actions to be taken by the robot corresponding to the states are listed in Table 4.1 and Table 4.2.

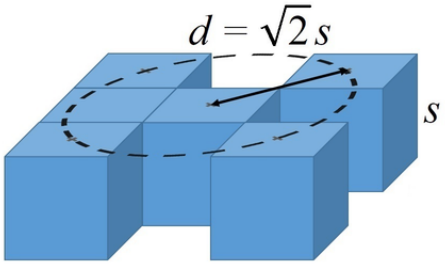

Fig. 4.3: The range for potentially coupled robots.

Table 4.1: States of robot R corresponding to distance *d* of the robot closest to R when *s* is the side length of robot.

Condition	State of R
$d \leq \sqrt{2}s$	United
$d > \sqrt{2}s$	Isolated

Table 4.2: Actions of robot R corresponding to states of R and distance *d* of the closest robot uncoupled to R ($d > \sqrt{2}s$) when *s* is the side length of robot.

State of R	Condition	Action of R
Isolated	$d = \infty$ (no robot detected)	Stay still
Isolated	$d > 3s$	Roll towards closest robot
Isolated	$\sqrt{2}s < d \leq 3s$	Jump towards closest robot
United	$d = \infty$ (only robots coupled to R detected)	Jump towards robots coupled to R in sequential order
United	$d > \sqrt{2}s$	Jump towards closest robot uncoupled to R

Rolling is the preferred way for an isolated robot to approach the other robots. While the path can be obstructed by other robots approaching it at the same time, rolling is performed when the distance to the closest robot is larger than 3s, as illustrated in Fig. 4.4. Otherwise, the robot approach the robot closest to it by jumping as a free path cannot be guaranteed. Example cases for two robots approaching each other by rolling and jumping are as shown in Fig. 4.5 and Fig. 4.6, where *t* indicates time.

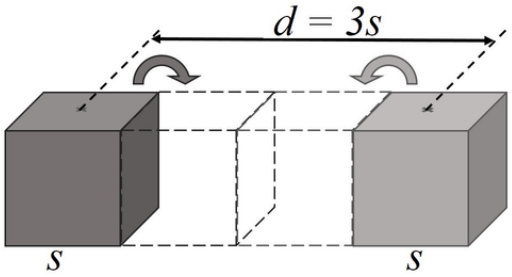

Fig. 4.4: The minimum separation for rolling action.

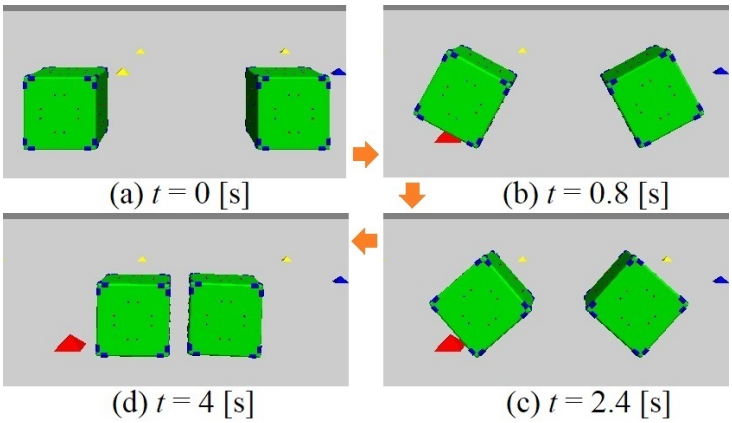

Fig. 4.5: Approach of two robots by rolling motion.

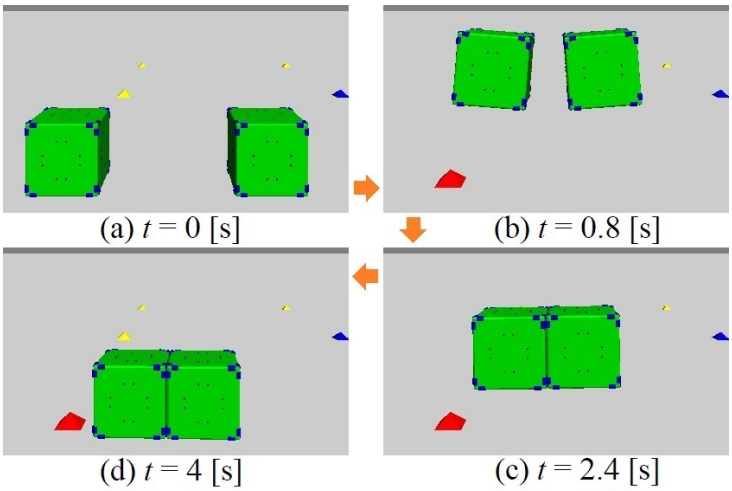

Fig. 4.6: Approach and coupling of two robots by jumping.

For a robot in united state, it is difficult for it to perform rolling effectively because probably at least one robot is in contact with it. In order to add more robot to the structure formed, the robot approaches other robots that are not coupled to it by jumping. To approach the other robot that is not coupled to it, the robot searches in all directions except top and bottom directions, for a robot closest to it in the range $d > \sqrt{2}s$, and jump towards that robot. If there is no robot detected besides of the robots coupled to it, it is impossible for the robot to determine the direction to advance in order to get more robots added to the structure with only local information. In such a case, the robot keep jumping towards the robots coupled to it in sequential order according to the rules.

When a robot jump forward, the angle is fixed at 67.5 degrees from the horizon, as illustrated

in Fig. 4.7. By doing so, all of the robots in the field are roughly at the same level at any instant during their jump, just as the two robots in Fig. 4.6, this maximize the possibility of robots to be coupled with the others.

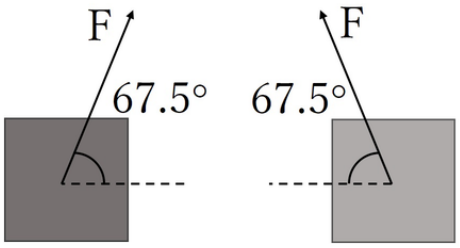

Fig. 4.7: Jumping of two robots at fixed angle towards each others.

4.3 Approach by rolling

To verify the effectiveness of the abovementioned rules in promoting coupling of robots in a field, especially on the case that robots were separated so far from the others and magnetic forces were too weak to pull robots together, mathematical expressions were used to prove that robots can approach the others by rolling, according to the rules.

To simplify the problem, the field with only two cubic robots, *robot A* and *robot B*, positioned far from each other on horizontal ground is considered, which is as shown in Fig. 4.8, and only *robot A* at the right side is focused. According to the abovementioned rules, it is known that the robot at A_0 will roll to A_1 in the next step and it is obvious that the displacement will be equal to the side length *s*.

Now, a polar coordinate system is considered with the centre of *robot B* as the origin *O*. Let *r* be the radial distance from the origin *O* to the centre of *robot A*, r_n be the length of *r* at time $t = n$, where r_0 be also the polar axis of the polar coordinate system, ϕ_n be the angle between r_n and the polar axis r_0 at time $t = n$, i.e. $\phi_0 = 0$.

The geometrical relationship of the robots at time $t = 0$ and time $t = 1$ is as shown in Fig. 4.8. When *robot A* at A_0 rolls to A_1, the centre of *robot A* moves from point (r_0, ϕ_0) to (r_1, ϕ_1). Let θ_0 be the angle as shown in Fig. 4.8. As robots always advance in the direction with smallest difference in angle to the polar axis, it is known that $\frac{-\pi}{4} \leq \theta_0 \leq \frac{\pi}{4}$. As it is assumed that the two

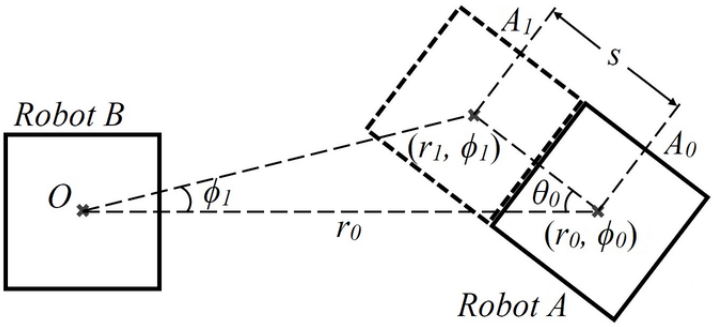

Fig. 4.8: Two robots positioned on horizontal ground.

robots are separated apart and performs rolling for approaching each other, $r_0 \geq 3s$ according to the rules. As $r_0 \geq 3s$ and the distance between A_0 and A_1 is s, it is known that $\frac{-\pi}{4} \leq \phi_1 \leq \frac{\pi}{4}$, and hence $\cos\phi_1 > 0$. From Fig. 4.8, the radii r_0 and r_1 satisfy

$$r_1 \cos\phi_1 = r_0 - s\cos\theta_0. \tag{4.1}$$

From Eq. (4.1) and $r_0 \geq 3s$, r_1 satisfies

$$r_1 = \frac{r_0 - s\cos\theta_0}{\cos\phi_1} \geq \frac{3s - s}{\cos\phi_1} \geq 2s. \tag{4.2}$$

When $\theta_0 = \phi_1 = 0$, Eq. (4.1) implies $r_1 = r_0 - s$, that is, $r_1 < r_0$. When $\theta_0 \neq 0$ and $\phi_1 \neq 0$, the sine formula gives the equality

$$\frac{s}{\sin\phi_1} = \frac{r_1}{\sin\theta_0} = \frac{r_0}{\sin(\pi - \theta_0 - \phi_1)}. \tag{4.3}$$

From Eq. (4.2) and the left side equality of Eq. (4.3), the inequality

$$\frac{\sin\theta_0}{\sin\phi_1} = \frac{r_1}{s} \geq 2 \tag{4.4}$$

is obtained. From the right side equality of Eq. (4.3), the equality

$$r_1 = \frac{\sin\theta_0}{\sin(\theta_0 + \phi_1)} r_0 \tag{4.5}$$

holds. From Eq. (4.4), θ_0 and ϕ_1 are of the same sign and satisfy the inequality $0 < |\phi_1| < |\theta_0| \leq \frac{\pi}{4}$. This implies that

$$\frac{\sin\theta_0}{\sin(\theta_0 + \phi_1)} < 1.$$

Therefore, from Eq. (4.5), $r_1 < r_0$ is satisfied.

The above discussion holds for any pair of robots in the field, and by substituing t_n and t_{n+1} by t_0 and t_1 respectively, it can be seen that the robots are approaching the other robots for every rolling action.

4.4 Simulation

4.4.1 The use of Open Dynamics Engine

The simulation was performed using Open Dynamics Engine (ODE) [48], which is a useful library for simulating rigid body dynamics, including functions for collision detection and drawing graphics. Because the simulation model can become unstable when objects collided with strong attraction force given by magnets, virtual spring and damper systems were implemented in the model, which activate when a pair of magnets were separated for less than four millimeters from contact.

4.4.2 Implementing Snap-through-buckling mechanisms

Since the robot to be included in the simulation model is based on Macrotis, interaction of robots can be better simulated by applying parameters close to the actual robot. Besides of basic parameters like size and weight of the robot, an experiment was conducted to measure the acceleration of the attached mass on the snap-through-buckling mechanism when triggered.

In the experiment, the mechanism was mounted on a fixed platform and the motion of the mass

attached on it was captured with a high-speed camera when the snap-through-buckling action was triggered. After that, the motion of the mass was analyzed using Tracker [49]. A cartesian coordinate system was defined on the platform with the x-axis aligned with the perpendicular bisector of the line joining the centers of the two shafts. The experimental setup is shown in Fig. 4.9.

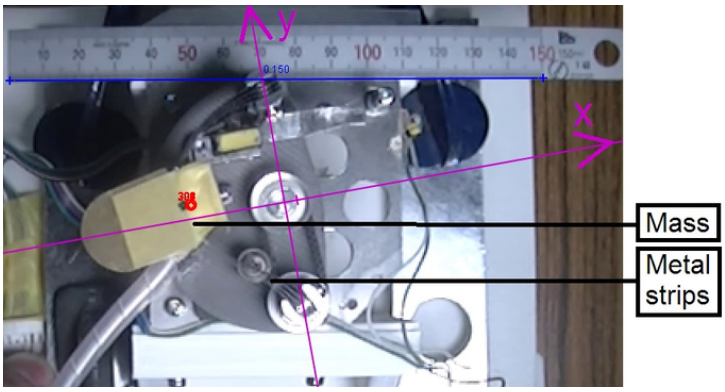

Fig. 4.9: The experimental setup on the snap-through-buckling mechanism.

For the current snap-through-buckling mechanism with only one drive shaft, it was observed that once snap-through-buckling action is triggered, the mass first accelerates in a direction 15 degrees deviated from the x-axis. Then an acceleration towards the y-axis can also be observed, where the maximum acceleration in the two directions occurred almost at the same instant. The displacement-time graph and acceleration-time graph in the x-direction are shown in Fig. 4.10 and Fig. 4.11 respectively; the acceleration-time graph in the y-direction is shown in Fig. 4.12.

From the results obtained, the estimated acceleration in the x and y directions are $159m/s^2$ and $84m/s^2$ respectively, which results in an acceleration of $180m/s^2$. The estimated deceleration in the x and y directions are $324m/s^2$ and $103m/s^2$ respectively. This results in a deceleration of $340m/s^2$ in a direction 1.7 degrees deviated from the abovementioned perpendicular bisector. Because the deceleration is stronger than the acceleration, there is a force pushing the mechanism in the forward direction overall.

After that, acceleration data that contribute most to the generation of force were extracted and an acceleration profile with 40 intervals was defined based on that. Note that the acceleration of the attached mass during actuation is considered to be constant according to the characteristic of the snap-through-buckling mechanism.

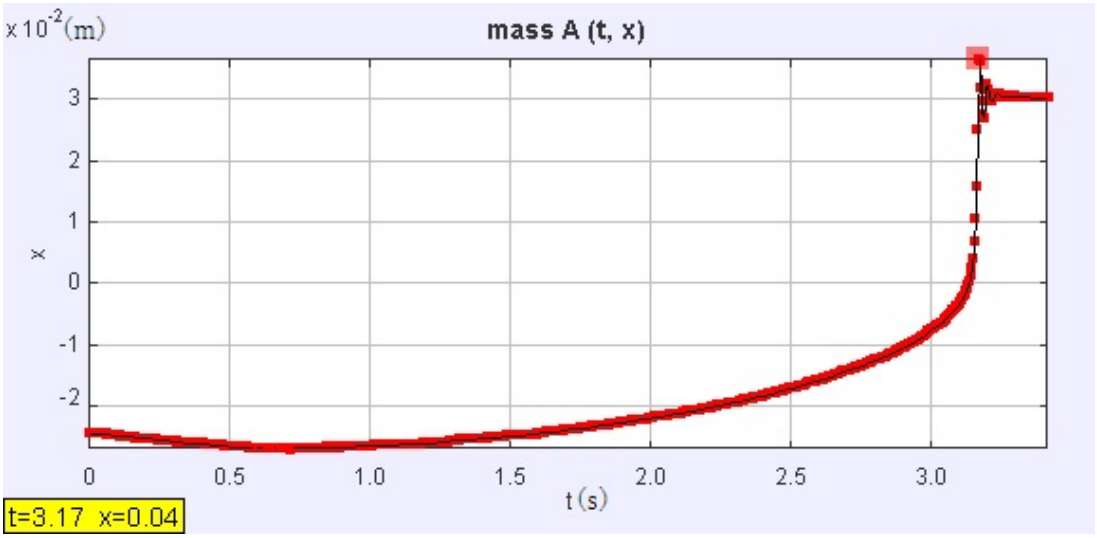

Fig. 4.10: Displacement of mass in x-direction against time.

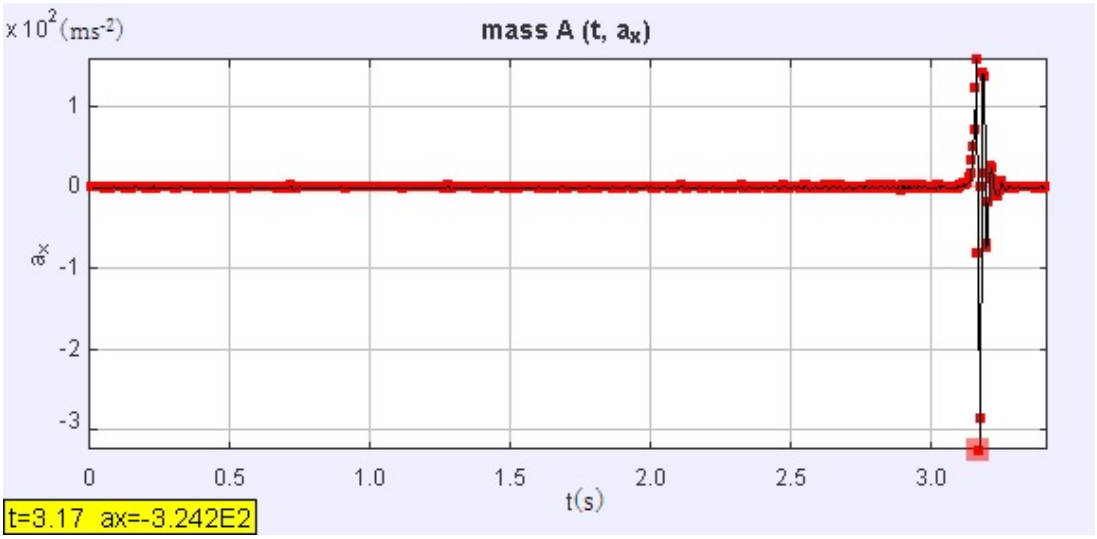

Fig. 4.11: Acceleration of mass in x-direction against time.

Then, according to the acceleration profile, forces to be generated by the two mechanisms at each simulation step were converted by the product of mass and acceleration, and the resultant translational force and torque acting on the robot were worked out for every simulation step, where duration of one simulation step is set as 2ms.

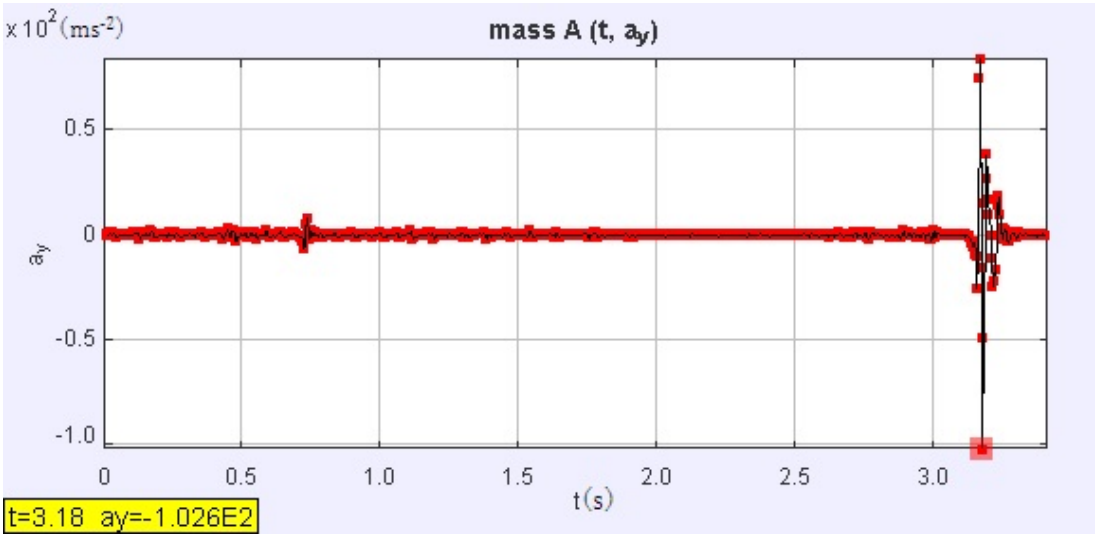

Fig. 4.12: Acceleration of mass in y-direction against time.

4.4.3 Calculation on magnets

To facilitate bonding between robots, cylindrical magnets and disc magnets are included on the robot. The properties of magnets are as shown in Table 4.3.

Table 4.3: Properties of magnets.

Properties	Value
Dimension of cylindrical magnets	$\phi 4 \times 15$ [mm]
Dimension of disc magnets	$\phi 4 \times 2$ [mm]
Residual magnetic flux density	1250 [mT]

For a magnet with radius *r*, length *l*, and residue magnetic flux density B_r, the magnetic moment can be calculated by

$$m = \frac{1}{\mu_0} B_r V, \tag{4.6}$$

where $\mu_0 = 4\pi \times 10^{-7}$ and $V = \pi r^2 l$.

After obtaining magnetic moments of magnets, force and torque acting on magnets located in the field can be calculated by using the equations that were applied in a previous study [50]. Eqs. (4.7) and (4.8) express the resultant force F_k and torque T_k respectively, acting on the magnetic moment m_k of *k*-th magnet cell located at position r_k, which is placed in the same field of other *N* magnet cells, with magnetic moment m_i and position r_i of *i*-th magnet cell.

$$F_k = \frac{\mu_0}{4\pi} \sum_{i=1}^{N} \frac{1}{|r_k - r_i|^4} \Bigg[-15 n_{ik}((m_k \cdot n_{ik})(m_i \cdot n_{ik})) \\ 3 n_{ik}(m_k \cdot m_i) + 3(m_k(m_i \cdot n_{ik}) + m_i(m_k \cdot n_{ik})) \Bigg] \tag{4.7}$$

$$T_k = \frac{\mu_0}{4\pi} \sum_{i=1}^{N} \frac{1}{|r_k - r_i|^3} \Big[3(m_k \times n_{ik})(m_i \cdot n_{ik}) - m_k \times m_i \Big] \tag{4.8}$$

where $n_{ik} = (r_k - r_i)/|r_k - r_i|$

Under current algorithm, torque and force between all pair of magnets on any two robots were calculated using nested loops and the results were summed up for each robot on each step. The workload can be heavy when the number of robots increases, where seventy-two magnets in total are included on one robot. To reduce workload, each magnet is represented by a single cell with the magnetic moment varied according to it's size, and the force and torque between a pair of cylindrical or disc magnets separated with a distance over three hundred millimeters are neglected, where the force between a pair of magnets separated with such a distance is lower than 2.60×10^{-6}N. To handle the massive computational requirement, magnetic force and torque are calculated in parallel using large-scaled computer systems OCTOPUS [51].

4.4.4 Assumptions

In the simulation, the environment is assumed to be a flat ground with micro gravity of $0.026G$, where *G* is the gravitational force on earth. All robots perform action in a perfectly synchronized regular interval. It is assumed that the robots can detect the direction of gravity (and so as the top side), the distance sensors are of infinity range but a robot cannot be detected by another robot with more than one sensor. Distance are measured with very high accuracy, and disturbance of signal does not exists.

4.4.5 Simulation results

In order to investigate the effectiveness of the proposed method for forming a structure, the number of clusters formed, the size of the largest cluster, and the number of steps required in the formation of structure with all robots included, were studied by using statistical methods. To investigate in how these criteria change when the number of robots increases, simulation was performed with 10, 20, 30 and 40 robots in the field, and each set was repeated with 20 cases of different initial position and orientation. Some simulation parameters and cases are listed in Tables 4.4 and 4.5 respectively. Although it can be observed that robots can reach the ground within 4s on a jump from Fig. 4.6, robots sometimes collide with other robots on a jump and take longer time to settle down. So, as shown in Table 4.4, the action period of robots was set as 8s to provide adequate time for the robots to settle down, so as to promote effective jumping and rolling.

Table 4.4: Parameters of the robot.

Parameter	Value
Side length s of robot	0.156 [m]
Total mass of robot	0.74 [kg]
Duration of a simulation step	2 [ms]
Robot's action period	8 [s]

Table 4.5: Simulation cases with different number of robots and dimensions of field

Case	1	2	3	4
Number of robots	10	20	30	40
Time limit [s]	400	800	1200	1200
Side length of field [m]	3.221	3.221	4.555	4.555
Field-robot side length ratio	20.645	20.645	29.196	29.196
Density [robot / m^2]	0.964	1.928	1.446	1.928

The results are as shown in Tables 4.6, 4.7, and 4.8. Note that 'S.D.' stands for standard deviation in all tables.

As shown in Table 4.6, it can be observed that clusters can be successfully formed in all cases, and the number of clusters formed increases in average with the number of robots in the field, where one cluster was formed in most of the cases with 10 robots, while two clusters were formed in average for cases with 40 robots.

From the minimum and average number of robots included in the largest cluster as shown in Table 4.7, it can be confirmed that the size of the largest cluster increases with the number of robots in the field.

Table 4.6: Statistics on number of clusters formed

Number of robots	Min.	Max.	Mean	S.D.
10	1	2	1.300	0.458
20	1	3	1.350	0.572
30	1	3	1.600	0.735
40	1	3	2.000	0.837

Table 4.7: Statistics on the number of robots in the largest cluster formed

Number of robots	Min.	Max.	Mean	S.D.
10	6	10	9.300	1.269
20	10	20	18.000	3.464
30	15	30	25.400	5.634
40	17	40	30.550	8.219

For those cases that one cluster was formed with all robots in the field, the time needed for forming the structures was analyzed, and the result is as shown in Table. 4.8. It can be seen that it takes more time for the formation of one cluster when the number of robots in the field is increased.

Examples showing the formation process of one cluster by 10, 20, 30 and 40 robots are as shown in Fig. 4.16, Fig. 4.17, Fig. 4.18 and Fig. 4.19 respectively, where t indicates time.

Table 4.8: Statistics on time (in seconds) needed for forming the cluster in the cases with all robots included in one cluster

Number of robots	Min.	Max.	Mean	S.D.
10	137.166	347.534	208.978	77.780
20	168.458	561.804	361.382	128.869
30	290.160	1150.946	537.428	310.486
40	362.784	857.394	570.604	151.732

Note that the size of the cluster formed may change if the time limit of a simulation case is extended. On the other hand, not all cases can have one cluster formed with all robots, even with infinite amount of time. An typical example of this is as shown in Fig. 4.13, where combination of the two clusters can hardly be achieved as the difference in orientation cannot be eliminated by letting the two clusters jumping towards and pushing each other even if the simulation continues.

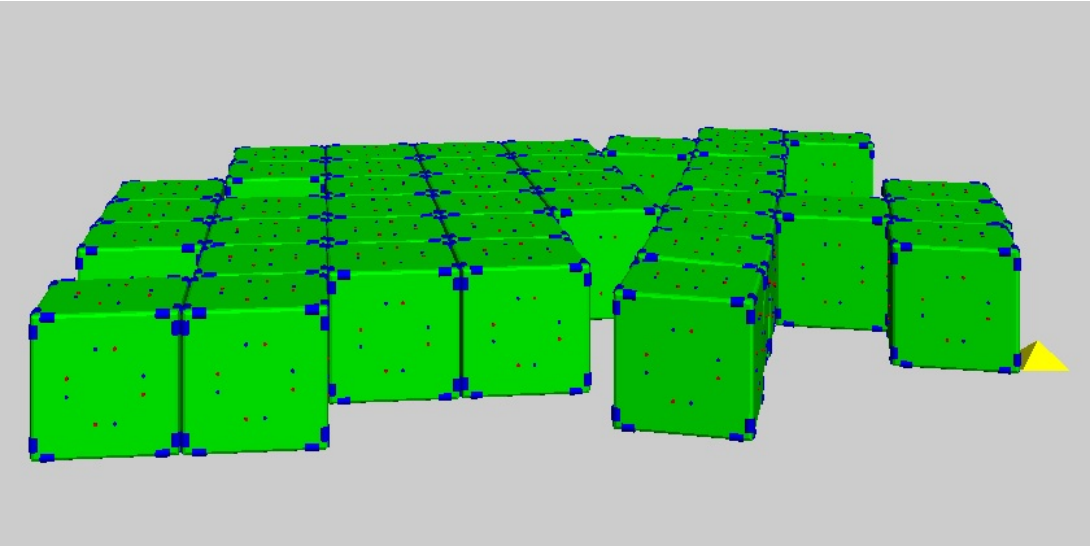

Fig. 4.13: An example showing that two clusters were formed with 40 robots.

In some cases, it is found that some robots were coupled with the clusters at the top instead of at the side, which are similar to the example as shown in Fig. 4.14, but because only a very small number of robots can do so, which is not more than three robots in all cases, the resultant structures formed are generally planar.

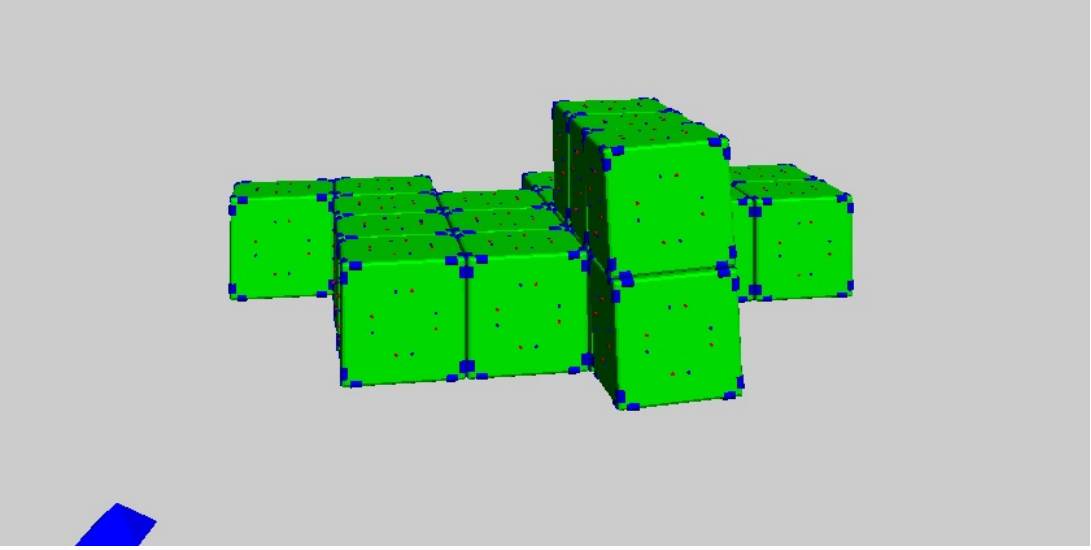

Fig. 4.14: An example showing that a cluster formed with robots at the top.

4.5 Discussion

In the current simulation, disturbance does not exist. For a group of robots placed on the ground at a particular initial position and orientation of all robots, the first step of action of all robots are predetermined. When the first step of action is executed, the dynamics of the robots, the interaction between the robots caused by the forces and torques between all magnets at every instant, and hence the final position and orientation of all robots at the end of first step are predetermined. Then, the second step of action of all robots are predetermined, just as the first step of action of all robots at a particular initial position and orientation, and it is obvious that the condition of the simulation model are predetermined for every step. So, it can be concluded that the size and shape of the resultant structure depend only on the intial position and orientation of all robots. This can be verified by the fact that the result of every test case is highly reproducible.

Consider the case as shown in Fig. 4.15, where a cluster of robots formed by *robot* C_1, *robot* C_2, *robot* C_3, *robot* C_4 and *robot* C_5, is approaching an isolated robot *robot D*.

According to the rules for robot's action, only *robot* C_1 and *robot* C_2 in the cluster generate forces directed to *robot D* as *robot D* can only be detected by them; the rest of the robots in the cluster, *robot* C_3, *robot* C_4 and *robot* C_5, generate forces to their neighbours in sequential order. This overall results a force that encourage the cluster of robots to approach *robot D*.

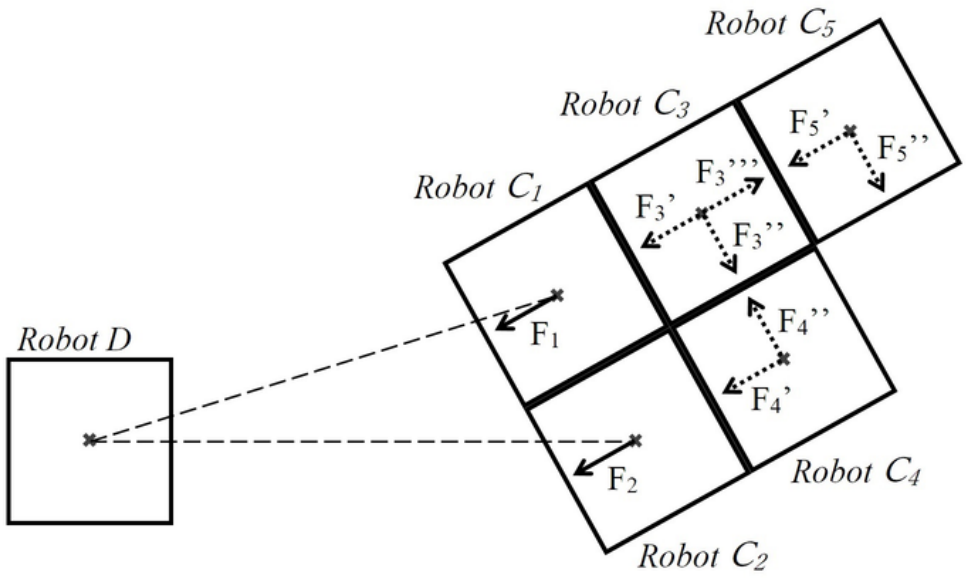

Fig. 4.15: A cluster of robot and an isolated robot approaching each other.

In this process, because the force for moving the whole cluster of robots towards *robot D* is contributed only by the robots at the side facing *robot D*, it is straightforward that the speed of migration generally decreases with the size of the structure. This explains why small clusters tend to approach large clusters, and the coupling of 2 large clusters for forming a single cluster at the end of the simulation always takes a long time.

Since the efficiency of clustering of robots decreaases when the size of cluster increases, advanced algorithm may be required to improve the efficiency when a giant structure is to be formed.

The difference between the simulation model and the real world is to be discussed below.

First, it is difficult to perfectly synchronize the action of all robots. There should be an error in the action timing for each robot. While robots can be highly synchronized by some simple communication method such as that proposed in the previous study [52], it is expected that the difference in timing can be minimized, and the minor difference in height between robots during a jump can be corrected by forces between magnets.

Second, for a robot measuring the distance of other robots with distance sensors at all faces, it is possible that the distance of the same robot were given by two neighboring sensors. There may be some difference in the action to be taken by robots, but this should not significantly affect the result because robots always move in the direction to another robot with minimum distance,

whether by rolling or jumping according to the rules.

Third, there should be an error between the actual centre-to-centre distance between two robots and the distance measured by the sensor on a face of a robot to another cube-shaped robot with varied orientation. While under the presence of measurement error, the robots were approaching the other robots whether by rolling or jumping under the rules, and the magnets help minimizing the position error when two robots come close.

4.6 Chapter concluding remarks

In this chapter, the idea of combining the actuator mechanisms of Macrotis with a body frame similar to that of M-block was suggested, and by applying the proposed rules, formation of planar structures by robots can be achieved. The effectiveness of the proposed rules in formation of structures were verified by conducting computer simulations.

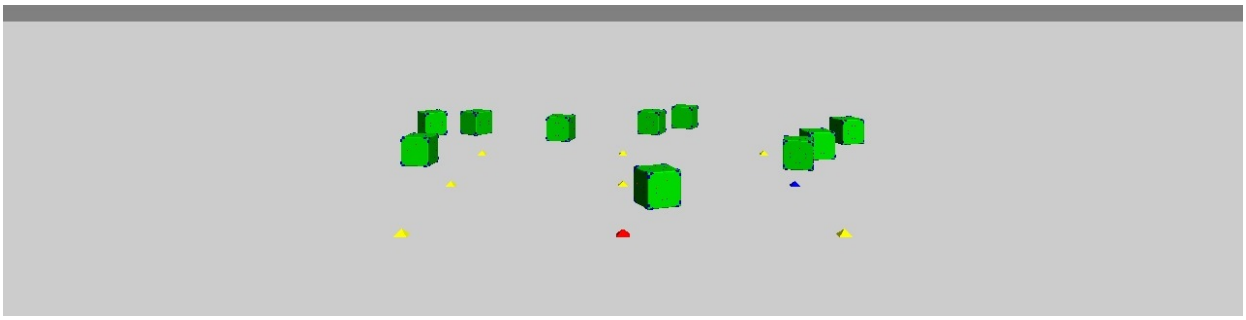

(a) $t = 0$ [s]

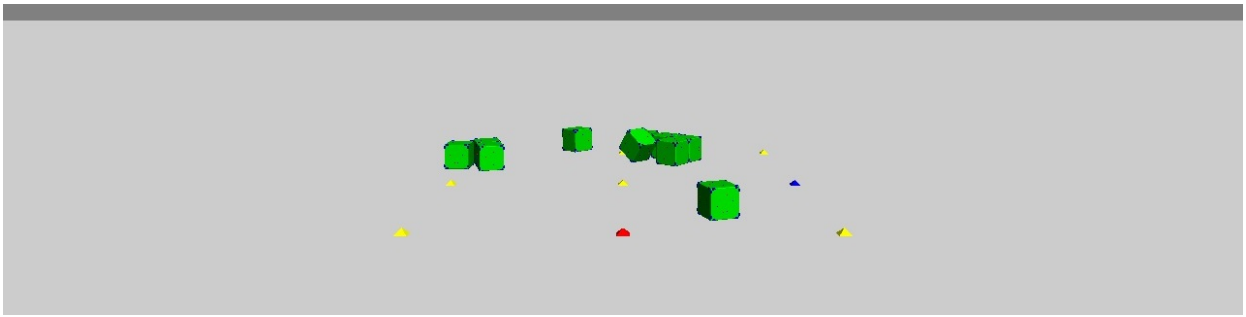

(b) $t = 46$ [s]

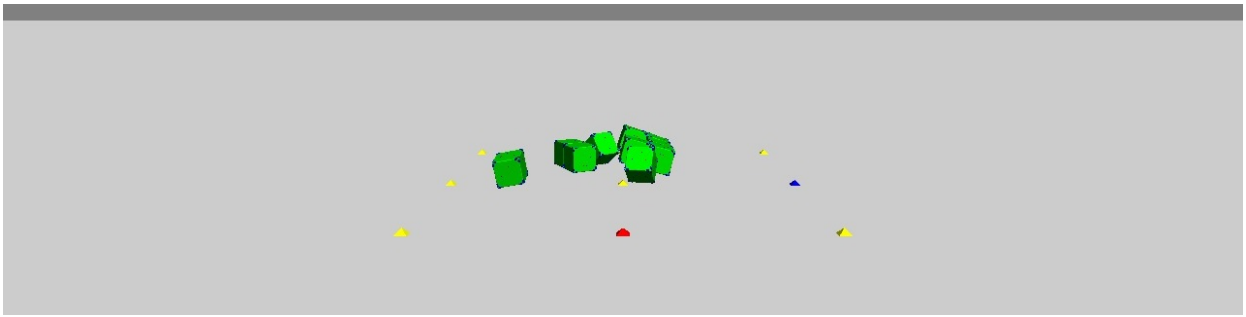

(c) $t = 92$ [s]

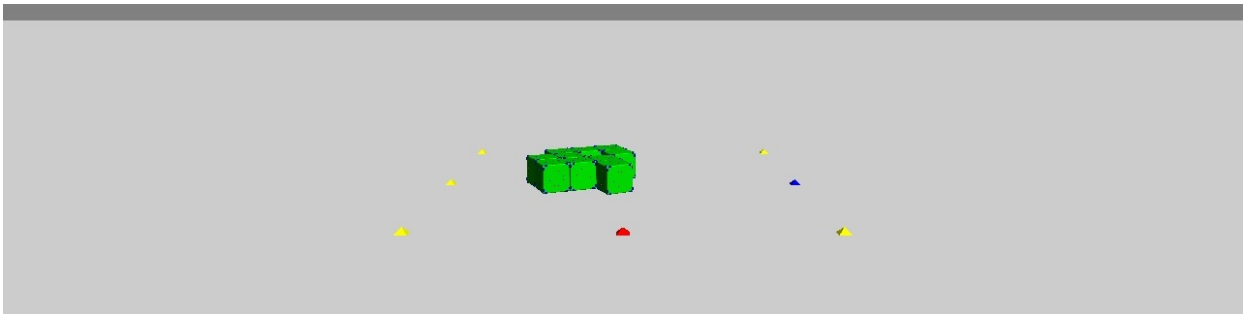

(d) $t = 184$ [s]

Fig. 4.16: An example showing the formation process of one cluster with 10 robots.

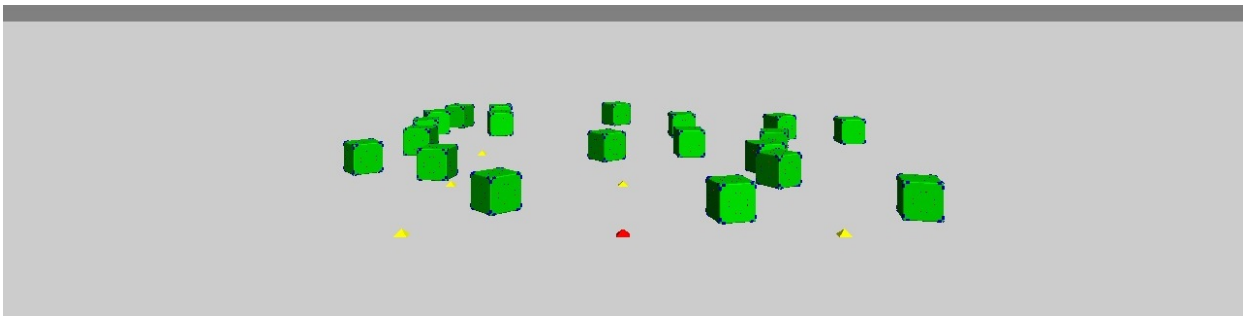

(a) $t = 0$ [s]

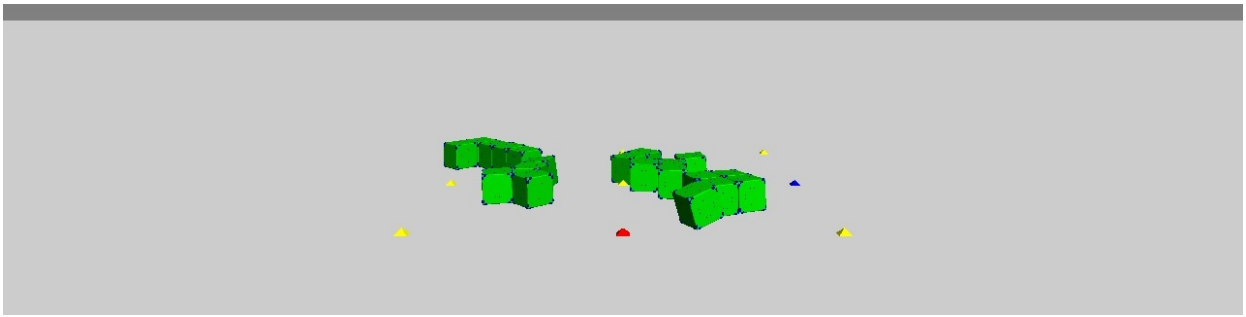

(b) $t = 84$ [s]

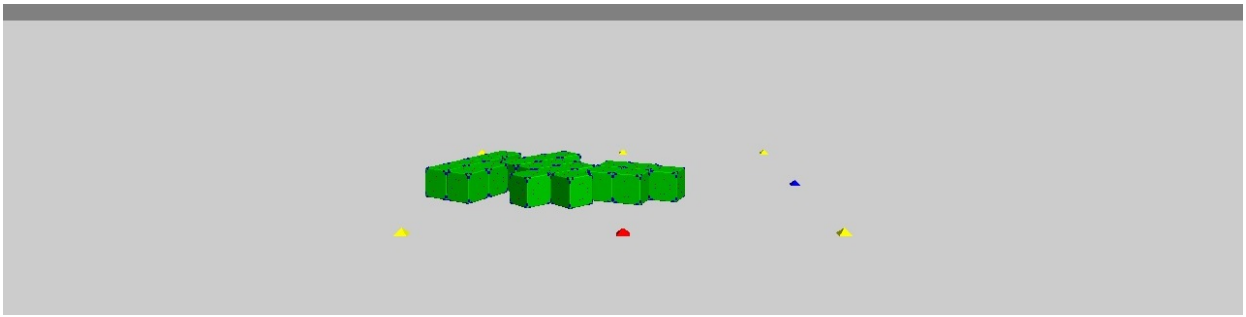

(c) $t = 168$ [s]

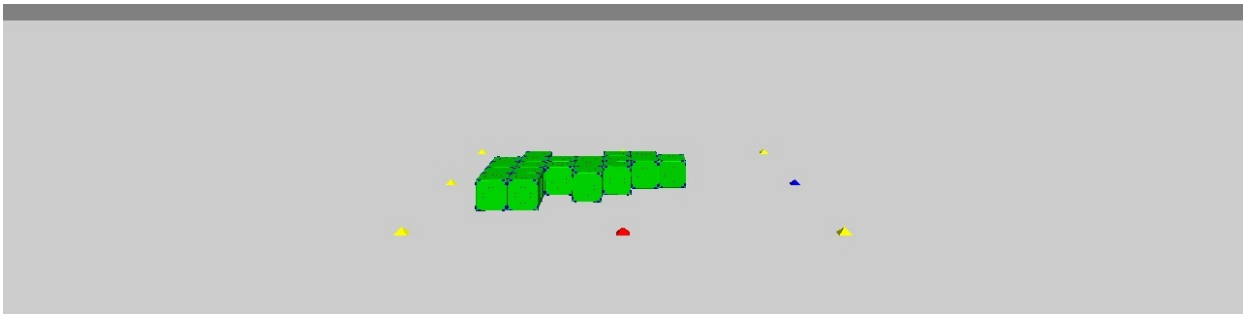

(d) $t = 336$ [s]

Fig. 4.17: An example showing the formation process of one cluster with 20 robots.

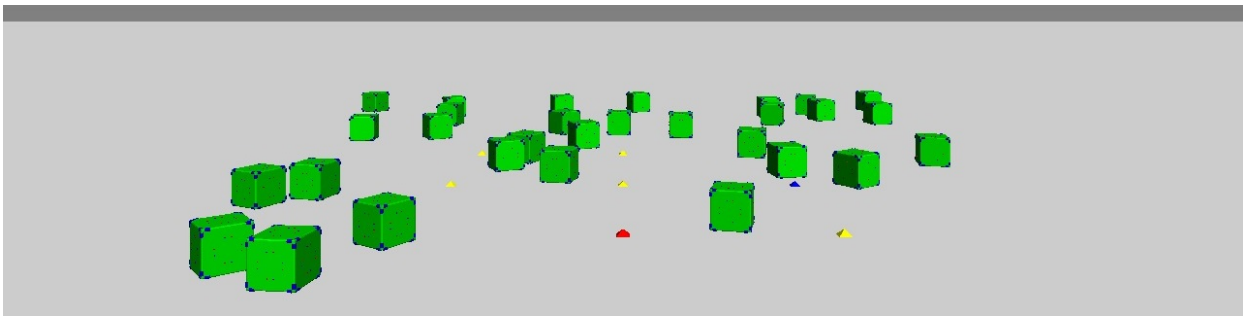

(a) $t = 0$ [s]

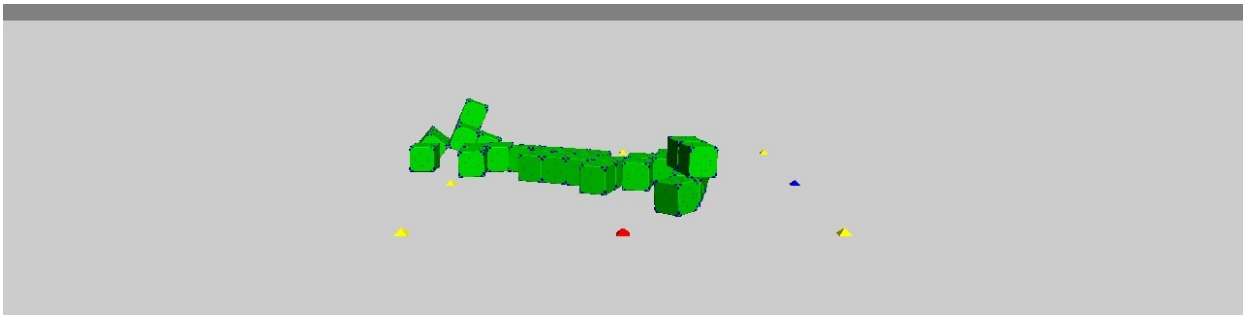

(b) $t = 150$ [s]

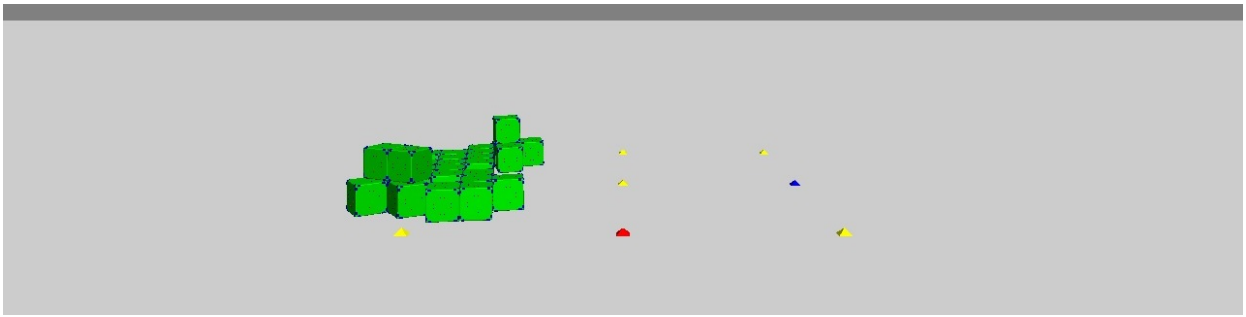

(c) $t = 300$ [s]

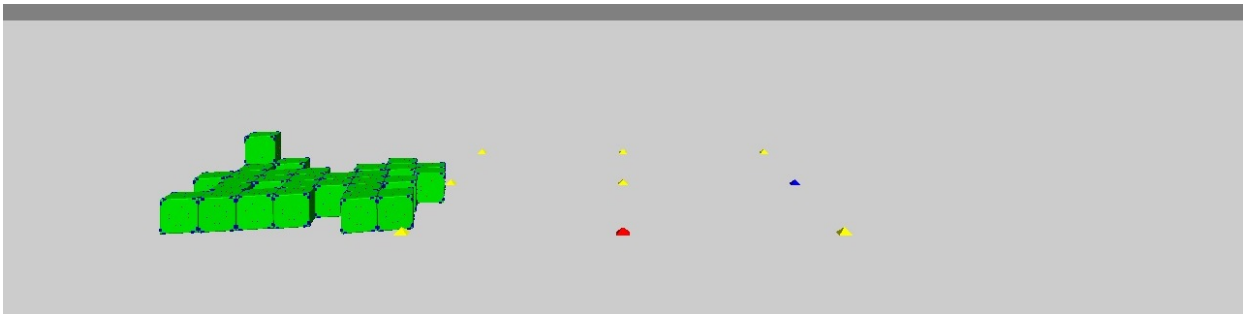

(d) $t = 600$ [s]

Fig. 4.18: An example showing the formation process of one cluster with 30 robots.

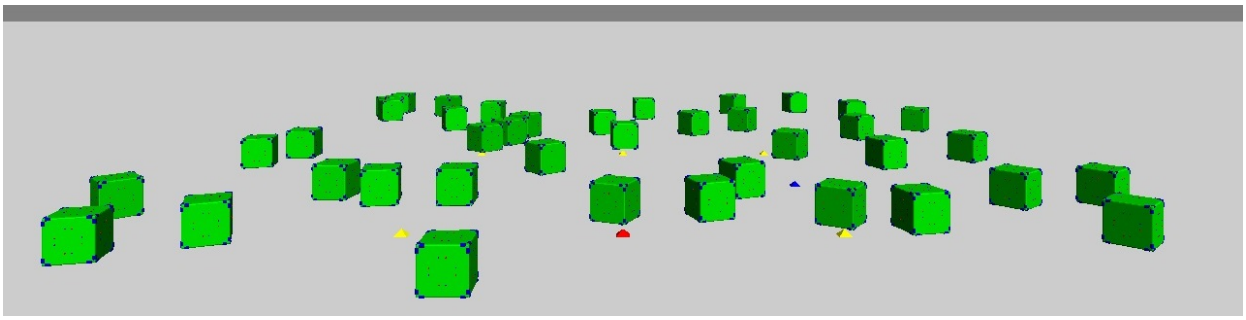

(a) $t = 0$ [s]

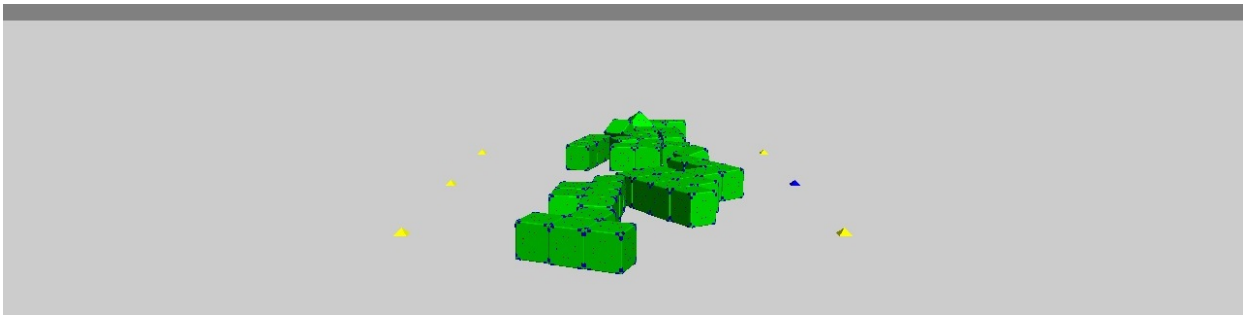

(b) $t = 150$ [s]

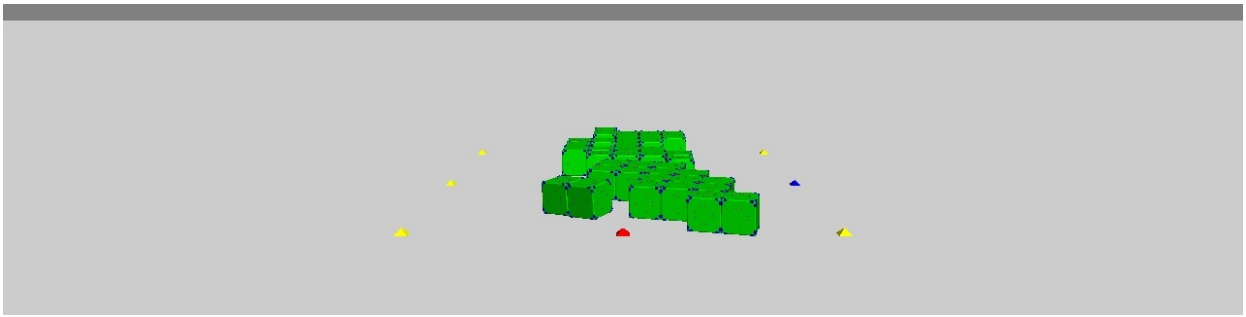

(c) $t = 300$ [s]

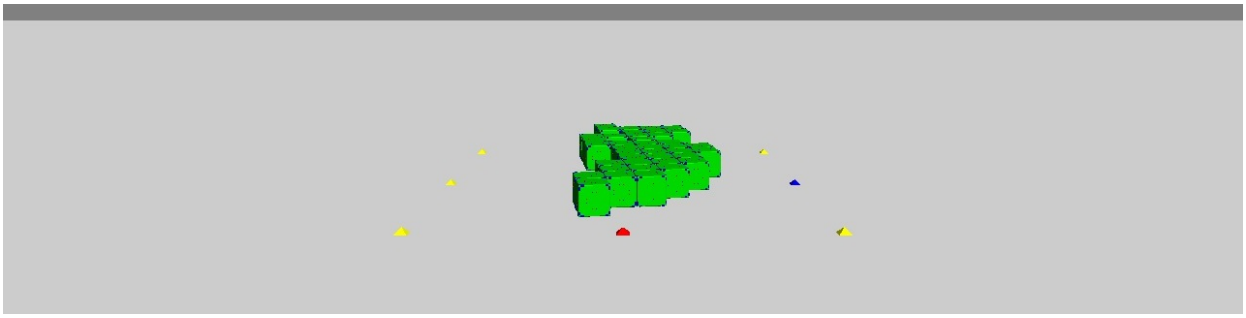

(d) $t = 600$ [s]

Fig. 4.19: An example showing the formation process of one cluster with 40 robots.

Chapter 5 Conclusion

5.1 Summary of dissertation

In chapter 2, the design of a newly developed cubic robot was revealed through mechanical and electronic aspects. Under the design, the robot is capable of rolling and jumping motions in multiple directions. Through experiments, the rolling and jumping motions of the robot under pseudo micro gravity environment were demonstrated.

In chapter 3, test modules equipped with platforms for wireless multi-master communication were produced, the design was then explained in structural and electronic aspects. Implementation of program for synchronization tests, including the configurations of identifier for the prioritization of message, was described. Through experiment with the test modules positioned in different formations, the performance of the proposed communication platform in synchronization of flashing was evaluated.

In chapter 4, the cubic robot which is equipped with actuator mechanisms of Macrotis and the body of M-block was considered. With the design, the robot is capable of rolling and jumping motions in multiple directions, and coupling with the other robots. Rules for controlling the rolling and jumping actions of such kind of robot were stated, where the effectiveness of distant robots on approaching the others under the rules was proven by using mathematical expressions. After measuring the acceleration of the attached mass on a triggered snap-through-buckling mechanism, acceleration data is implemented into a computer simulation model using ODE, which was used for calculating force and torque produced by robots. Together with the formulae for resolving force and torque on a pair of magnets, computer simulations were conducted with cases of different number of robots, at different initial position and orientation in the field. The effectiveness of the rules in formation of structures by the new modular robot was verified.

5.2 Conclusion and future work

In this thesis, a new cubic modular robot system was designed. By applying snap-through-buckling mechanisms, the robot can achieve a high freedom of movement and can support rolling and jumping motions without concerning the orientation of the robot. The rolling and jumping performance of the robot under pseudo micro gravity environment have been confirmed in experiments. Also, a multi-master communication platform was developed, which allows communication to be established between randomly positioned distributed systems. With the suggested priority scheme using the identifier, synchronized action was achieved on distributed systems. This is beneficial to decentralized control of distributed systems. With highly synchronized actions achievable on cubic modular robots of high freedom of movement, a simple algorithm was developed for the formation of structure with the modular robots. A computer simulation were conducted based on the cubic modular robot, and it is shown that planar structures can be successfully constructed with the modular robots under a synchronized decentralized control.

With the effectiveness of the proposed modular robot system on the formation of structure demonstrated in the study, more studies can be carried out in the future so as to increase the functionality and usability of the system, which can eventually put the modular robot system into actual use. To achieve this goal, the actuator mechanism has to be improved, to allow generation of higher and adjustable output power, such that the modular robot system can be applied in various environment with different gravity. If the robot can attain adequate output power to perform similar motion on earth, experiment can be conducted on actual robots with magnets installed. Moreover, if the robots have adequate power to stack over other robots, control algoritm can be considered to allow formation of structure of different shape besides of planar structures. Similar algorithms can also be considered for surrounding an object with modular robots, so as to increase the stability, and also to allow transportation of objects.

For the locomotion of structure, an even field has been considered in current setting. It should be interesting to investigate on the interaction of the robots with an uneven field, so as to allow the robots to be applied in different areas.

Reference

[1] B. Budianshky, B. Mantlo, R. Macchio, and J. Salicrup, “Transformers”, Marvel, United States, 1984.

[2] J. Cameron, and W. Wisher, “Terminator 2:Judgement Day”, 1991.

[3] H. Arakawa, “Fullmetal Alchemist”, 2001.

[4] D. Hall, and C. Williams, “Big Hero 6”, Walt Disney Animation Studios, 2014.

[5] T. Fukuda, and S. Nakagawa, “Approach to the dynamically reconfigurable robotic system”, Journal of Intelligent and Robotic Systems, Vol. 1, No. 1, pp. 55-72, Springer, 1988.

[6] K. Gilpin, and D. Rus, “Modular robot systems”, IEEE Robotics & Automation Magazine, Vol. 17, No. 3, pp. 38-55, 2010.

[7] A. Castano, W.M. Shen, and P. Will, “CONRO: Towards deployable robots with inter-robots metamorphic capabilities”, Autonomous Robots, Vol.8, No.3, pp. 309-324, Springer, 2000.

[8] H. Kurokawa, K. Tomita, A. Kamimura, E. Yoshida, S. Kokaji, and S. Murata, “Distributed self-reconfiguration control of modular robot m-tran”, Mechatronics and Automation, 2005 IEEE International Conference, Vol.1, pp. 254-259, 2005.

[9] Y. Suzuki, N. Inou, H. Kimura, and M. Koseki, “Reconfigurable group robots adaptively transforming a mechanical structure -numerical experssion of criteria for structural transformation and automatic motion planning method”, Intelligent Robots and Systems (IROS), 2007 IEEE/RSJ International Conference on, pp. 2361-2367, 2007.

[10] M. W. Jorgensen, E. H. Ostergaard, and H. H. Lund, “Modular ATRON: Modules for a self-reconfigurable robot”, Intelligent Robot and Systems (IROS), 2004 IEEE/RSJ International Conference on, Vol.2, pp. 2068-2073, IEEE, 2004.

[11] J. W. Romanishin, K. Gilpin, and D. Rus, “M-blocks: Momentum-driven, magnetic modular robots”, Intelligent Robots and Systems (IROS), 2013 IEEE/RSJ International Conference on, pp. 4288-4295, 2013.

[12] T. Hirano, M. Ishikawa, and K. Osuka, “Control and development of cylindrical mobile robot”, Journal of Robotics and Mechatronics, Vol.25, No.2, pp. 392-399, Fuji Technology Press Ltd., 2013.

[13] A. Fujiwara, J. Kawaguchi, D. K. Yeomans, M. Abe, T. Mukai, T.Okada, J. Saito, H. Yano, M. Yoshikawa, D. J. Scheeres, and others, “The rubble-pile asteroid Itokawa as observed by Hayabusa”, Science, Vol.312, No.5778, pp. 1330-1334, American Association for the Advancement of Science, 2006.

[14] T. G. Müller, J. Ďurech, M. Ishiguro, M. Mueller, T. Krühler, H. Yang, M. J. Kim, L. O’ Rourke, F. Usui, C. Kiss, and others, “Hayabusa-2 mission target asteroid 162173 Ryugu (1999 JU3): Searching for the object’ s spin-axis orientation”, Astronomy & Astrophysics, Vol.599, A103, EDP Science, 2017.

[15] Website for Curiosity Rover, https://mars.nasa.gov/msl/

[16] T. Yoshimitsu, “”Development of autonomous rover for asteroid surface exploration”, Robotics and Automation, 2004. Proceedings. ICRA’04. IEEE International Conference on, Vol.3, pp. 2529-2534, IEEE, 2004.

[17] J. Reill, H. J. Sedlmayr, P. Neugebauer, M. Maier, E. Krämer, and R. Lichtenheldt, “MASCOT - asteroid lander with innovative mobility mechanism”, ASTRA, 2015.

[18] “’Hedgehog’ Robots Hop, Tumble in Microgravity”, Jet Propulsion Laboratory- California Institute of Technology, 3 September, 2015. https://www.jpl.nasa.gov/news/news.php?feature=4712 [accessed Nov. 21, 2018]

[19] K. Ohgata, K. Osuka, K. Tadakuma, H. Mochiyama, and M. Bando, “On acutator unit for asteroid exploration rover using buckling phenomenon”, Proceedings of the Space Science and Technology Conference, 57 (2013) 4p. (In Japanese)

[20] T. B. A. Lastrilla, K. Osuka, Y. Sueoka, and Y. Sugimoto, “Design Proposal for a Small Asteroid Surface Rover HORUS”, The 3rd Multi-symposium on Control Systems(MSCS), CD, 2D3-5, 2016.

[21] Website: Development of small asteroid exploration rover MINERVA-II (In Japanese), $https://www.osaka-u.info/wp-content/uploads/2019/08/top_article_3-13.pdf$ [accessed Oct. 25, 2019]

[22] Website: Hayabusa 2 Has Sent its Last Rover to Ryugu, https://www.universetoday.com/143643/hayabusa-2-has-sent-its-last-rover-to-ryugu/ [accessed Oct. 25, 2019]

[23] S. Kernbach, Handbook of Collective Robotics: Fundamentals and Challenges, Pan Stanford Publishing Pte. Ltd., USA, 2013.

[24] R. W. Moses, and D. M. Bushnell, "Frontier in-situ resource utilization for enabling sustained human presence on mars", NAXA, 2016.

[25] K. J. Kennedy, "The vernacular of space architecture", AIAA Space Architecture Symposium, pp. 6102, 2002.

[26] J. Banik, and T. Murphey, "Performance validation of the triangular rollable and collapsible mast", *AIAA/USU 24th Conference on Small Satellites*, SSC10II-1, pp. 1-8, 2010.

[27] E. R. Adrover, Deployable structures, Laurence King Publishing Ltd., London, 2015.

[28] S. A. Zirbel, S. P. Magleby, L. L. Howell, R. J. Lang, M. W. Thomson, D. A. Sigel, P. E. Walkemeyer, B. P. Trease, "Accommodating thickness in origami-based deployable arrays", Journal of Mechanical Design, Vol.135, No.11, American Society of Mechanical Engineerings, 2013.

[29] I. Navarro, and F. Matía., "An introduction to swarm robotics." Isrn robotics 2013, 2012.

[30] P. E. Rybski, A. Larson, H. Veeraraghavan, M. LaPoint, and M. Gini, Distributed Autonomous Robotic Systems 6, pp. 317-326, Springer, 2007.

[31] S. Corrigan, "Introduction to the controller area network (CAN)." Texas Instrument, Application Report, 2008.

[32] M. Yim, D. G. Duff, and K. D. Roufas, "PolyBot: a modular reconfigurable robot." Robotics and Automation, 2000. Proceedings. ICRA'00. IEEE International Conference on, Vol.1, pp. 514-520, IEEE, 2000.

[33] H. Wei, Y. Chen, J. Tan, and T. Wang, "Sambot: A self-assembly modular robot system" IEEE/ASME Transactions on Mechatronics, Vol.16, No.4, pp. 745-757, IEEE, 2011.

[34] M. Mikawa, “Robust Wireless Communication for Small Exploration Rovers Equipped with Multiple Antennas by Estimating Attitudes of Rovers in Several Experimental Environments.” *Journal of Robotics and Mechatronics*, Vol.29, No.5, pp. 864-876, Fuji Technology Press Ltd., 2017.

[35] Y. L. Liao, and K. L. Su, “Multi-robot-based intelligent security system” Artificial Life and Robotics, Vol.16, No.2, pp. 137, Springer, 2011.

[36] S. Jiang, J. Cao, Y. Liu, J. Chen, and X. Liu, “Programming large-scale multi-robot system with timing constraints” Computer Communication and Networks (ICCCN), 2016 25th International Conference on, pp. 1-9, IEEE, 2016.

[37] Á. Gutiérrez, A. Campo, M. Dorigo, J. Donate, F. Monasterio-Huelin, and L. Magdalena, “Open E-puck Range & Bearing Miniaturized Board for Local Communication in Swarm Robotics” Robotics and Automation, 2009. ICRA’09. IEEE International Conference on., pp. 3111-3116, IEEE, 2009.

[38] J. McLurkin, J. Rykowski, M. John, Q. Kaseman, and A. J. Lynch, “Using multi-robot systems for engineering education: Teaching and outreach with large numbers of an advanced, low-cost robot” IEEE Transactions on Education, Vol.56, No.1, pp. 24-33, IEEE, 2013.

[39] M. Rubenstein, C. Ahler, and R. Nagpal, “Kilobot: A low cost scalable robot system for collective behaviors” Robotics and Automation (ICRA), 2012 IEEE International Conference on, pp. 3293-3298, IEEE, 2012.

[40] I. Illgen, H. Schrom, and E. Schnieder., “Infrared CAN Interface - Principles of CAN data transmission using infrared light.” Proceedings of the 7th International CAN Conference (iCC). 2000.

[41] S. Camazine, J. L. Deneubourg, N. R. Franks, J. Sneyd, G. Theraulaz, E. Bonabeau, Self-organization in biological systems. Vol. 7. Princeton University Press, 2003.

[42] F. Hartwich, and A. Bassemir., “The configuration of the CAN bit timing.” 6th International CAN Conference. 1999.

[43] A. Yamada, H. Mochiyama, and H. Fujimoto, “Statics analysis of the robotic catapults based on the closed elastica”, Journal of the Robotics Society of Japan, Vol.26, No.2, pp. 169-177, 2008. (In Japanese)

[44] Website for Mbed LPC 1768 microcontroller board, https://os.mbed.com/platforms/mbed-LPC1768/ [accessed Feb. 20, 2019]

[45] D. Payton, R. Estkowski, and M. Howard., "Compound behaviors in pheromone robotics." Robotics and Autonomous Systems Vol.44, No.3-4, pp. 229-240, 2003.

[46] K. Mak, K. Osuka, Y. Sugimoto and T. Wada, "MACROTIS: cubic robot with snap-through-buckling mechanisms for achieving high freedom of movement", *Journal of Robotics and Mechantronics*, Vol.31, No.3, pp. 500-506, Fuji Technology Press Ltd., 2019.

[47] T. Hirano, M. Ishikawa and K. Osuka, "Control and Development of Cylindrical Mobile Robot," *Journal of Robotics and Mechantronics*, Vol.25, No.2, pp. 392-399, Fuji Technology Press Ltd., 2013.

[48] ODE Website, https://www.ode.org/

[49] Website for Tracker, https://physlets.org/tracker/ [accessed Nov. 21, 2018]

[50] B. Thomaszewski, A. Gumann, S. Pabst, and W. Straßer, "Magnets in motion," *ACM Transactions on Graphics (TOG)*, Vol.27, No.5, pp. 162, ACM, 2008.

[51] OCTOPUS Website, http://www.hpc.cmc.osaka-u.ac.jp/en/octopus/

[52] K. Mak, K. Osuka and T. Wada, "Development of a Multi-Master Communication Platform for Mobile Distributed Systems", *Journal of Robotics and Mechantronics*, Vol.31, No.2, pp. 348-354, Fuji Technology Press Ltd., 2019.

List of publications

Journal papers

1. K. Mak, K. Osuka and T. Wada, “Development of a Multi-Master Communication Platform for Mobile Distributed Systems”, *Journal of Robotics and Mechantronics*, Vol.31, No.2, pp. 348-354, Fuji Technology Press Ltd., 2019.

2. K. Mak, K. Osuka, Y. Sugimoto and T. Wada, “MACROTIS: cubic robot with snap-through-buckling mechanisms for achieving high freedom of movement”, *Journal of Robotics and Mechantronics*, Vol.31, No.3, pp. 500-506, Fuji Technology Press Ltd., 2019.

International conference

1. K. Mak, K. Osuka and T. Wada, “Formation of planar structures with rollable and jumpable cubic modular robots”, *Proceedings of the 3rd International Symposium on Swarm Behavior and Bio-Inspired Robotics*, pp. 114-120, USB flash drive, Okinawa, Japan, 20-22 November, 2019.

2. K. Mak, K. Osuka, Y. Sugimoto and T. Wada, “Design of cubic robot for achieving high freedom of movement with the use of snap-through-buckling mechanism”, *Proceedings of the SICE Annual Conference 2018*, pp. 1551-1554, Nara, Japan, 11-14 September, 2018.

Domestic conference

1. K. Mak, K. Osuka, Y. Sugimoto and T. Wada, “Design of a reconfigurable robot MACRO-TIS for exploration on small asteroids”, *Proceedings of 62th Space Sciences and Technology Conference*, CD, 3I01, Fukuoka, Japan, 24-26 October, 2018.

2. K. Mak and K. Osuka, “A study on the use of snap-through-buckling mechanism for the locomotion of robot”, *23rd Emergent System Symposium*, P15, Nagano, Japan, 8-10 September, 2017.

3. K. Mak and N. Maru, “Landing control of a quadcopter by using visual-space based visual servoing”, *Proceedings of 16th System Integration Division Annual Conference(SI2015)*, pp. 482-487, Nagoya, Japan, 14-16 December, 2015.